

Review

Trojan Horse Investigation for AGB Stellar Nucleosynthesis

Maria Letizia Sergi ^{1,2,*} , Giuseppe D'Agata ³ , Giovanni Luca Guardo ², Giuseppe Gabriele Rapisarda ^{1,2} ,
Vaclav Burjan ³, Silvio Cherubini ^{1,2}, Marisa Gulino ^{2,4} , Iolanda Indelicato ², Marco La Cognata ² ,
Livio Lamia ^{1,2,5} , Dario Lattuada ^{2,4} , Jaromir Mrázek ³, Alessandro Alberto Oliva ^{1,2},
Rosario Gianluca Pizzone ² , Stefano Romano ^{1,2,5}, Roberta Spartá ² , Oscar Trippella ⁶ and Aurora Tumino ^{2,4}

- ¹ Dipartimento di Fisica e Astronomia "Ettore Majorana", Università degli Studi di Catania, 95123 Catania, Italy; grapisarda@lns.infn.it (G.G.R.); cherubini@lns.infn.it (S.C.); llamia@lns.infn.it (L.L.); aoliva@lns.infn.it (A.A.O.); romano@lns.infn.it (S.R.)
- ² Laboratori Nazionali del Sud, Istituto Nazionale di Fisica Nucleare, 95123 Catania, Italy; guardo@lns.infn.it (G.L.G.); gulino@lns.infn.it (M.G.); indelicatoiolanda@gmail.com (I.I.); lacognata@lns.infn.it (M.L.C.); lattuada@lns.infn.it (D.L.); rgpizzone@lns.infn.it (R.G.P.); rsparta@lns.infn.it (R.S.); tumino@lns.infn.it (A.T.)
- ³ Nuclear Physics Institute of the Czech Academy of Sciences, 250 68 Řež, Czech Republic; peppeddagata@gmail.com (G.D.); burjan@ujf.cas.cz (V.B.); mrazek@ujf.cas.cz (J.M.)
- ⁴ Facoltà di Ingegneria e Architettura, Università degli Studi di Enna "Kore", 94100 Enna, Italy
- ⁵ Centro Siciliano di Fisica Nucleare e Struttura della Materia, CSFNSM, 95123 Catania, Italy
- ⁶ INFN Perugia, 06123 Perugia, Italy; oscartrippella@gmail.com
- * Correspondence: marialetizia.sergi@dfa.unict.it

Abstract: Asymptotic Giant Branch (AGB) stars are among the most important astrophysical sites influencing the nucleosynthesis and the chemical abundances in the Universe. From a pure nuclear point of view, several processes take part during this peculiar stage of stellar evolution thus requiring detailed experimental cross section measurements. Here, we report on the most recent results achieved via the application of the Trojan Horse Method (THM) and Asymptotic Normalization Coefficient (ANC) indirect techniques, discussing the details of the experimental procedure and the deduced reaction rates. In addition, we report also on the on going studies of interest for AGB nucleosynthesis.

Keywords: nuclear astrophysics; AGB nucleosynthesis; indirect methods



Citation: Sergi, M.L.; D'Agata, G.; Guardo, G.L.; Rapisarda, G.G.; Burjan, V.; Cherubini, S.; Gulino, M.; Indelicato, I.; La Cognata, M.; Lamia, L.; et al. Trojan Horse Investigation for AGB Stellar Nucleosynthesis. *Universe* **2022**, *8*, 128. <https://doi.org/10.3390/universe8020128>

Academic Editor: John Martin

Received: 16 December 2021

Accepted: 12 February 2022

Published: 16 February 2022

Publisher's Note: MDPI stays neutral with regard to jurisdictional claims in published maps and institutional affiliations.



Copyright: © 2022 by the authors. Licensee MDPI, Basel, Switzerland. This article is an open access article distributed under the terms and conditions of the Creative Commons Attribution (CC BY) license (<https://creativecommons.org/licenses/by/4.0/>).

1. Introduction

The Asymptotic Giant Branch (AGB) phase is the evolved stage of stars with $M \leq 6 M_{\odot}$ and is of critical importance for nucleosynthesis. Stars with $M > 6 M_{\odot}$ and up to 9–10 M_{\odot} climb the AGB too and they are usually called super AGBs. This phase is characterized by nuclear burning of hydrogen and helium in shells surrounding the electron-degenerate core of carbon and oxygen (or for the most massive superAGB stars, a core of oxygen, neon, and magnesium). The radiative burning of the H-shell provides energy to the star for most of the time. Its activity is interrupted by recurrent thermonuclear flashes induced by the convective burning of the He-shell (and of the C-shell in the case of the more massive superAGBs). Such a stratified structure going through alternating phases of burning (radiative and convective) is also affected by a mixing phenomena, which not only enrich the stellar envelope of fresh nucleosynthesis products but also allow particular nucleosynthesis processes to take place [1].

AGB stars play a major role in determining the galactic chemical evolution being the production site of almost 50% of elements heavier than iron through the slow neutron capture process (the so-called s-process). The s-nucleosynthesis path runs along the stability valley due to the competition between n-captures and β -decays [2]. In particular, several stable nuclei with masses between 90 and 209 belong to the main component of the s-process

and are synthesized by AGB stars thanks to the neutrons delivered by the $^{13}\text{C}(\alpha, n)^{16}\text{O}$ and $^{22}\text{Ne}(\alpha, n)^{25}\text{Mg}$ reactions.

The main source of neutrons in AGB with $M < 3 M_{\odot}$ is the $^{13}\text{C}(\alpha, n)^{16}\text{O}$ reaction, which is burnt in a reservoir of ^{13}C in the He-rich layers below the H shell, when the last is active [3]. The modeling of the formation of this ^{13}C reservoir, called the ^{13}C pocket, is among the most debated and uncertain topics on AGB stars. Several models have been so far presented in the literature, from more simplified and parametric ones to the most complex one based on multidimensional hydrodynamic approaches. Comparing the results of such models would deserve a devoted paper. However, since our contribution is dealing with the experimental measurement of nuclear reactions, we limit ourselves to describing the formation of the ^{13}C pocket in the most simplified way.

At the end of the convective He-burning episodes (when instead the $^{22}\text{Ne}(\alpha, n)^{25}\text{Mg}$ possibly operates), a convective phenomenon, known as third dredge-up (TDU), runs over the regions below the envelope down to the He-burning shell and brings into the stellar surface the nucleosynthesis products. During the TDU, proton-rich materials penetrate the bottom edge of the convective zone down to the stellar layers rich in ^{12}C and ^4He , which are below the H-shell. When this latter returns to burn the injected protons, it allows for the formation of the so-called ^{13}C -pocket through the $^{12}\text{C}(\text{p}, \gamma)^{13}\text{N}(\beta^+ \nu)^{13}\text{C}$ reaction chain, and then, thanks to the abundance of α particles, the $^{13}\text{C}(\alpha, n)^{16}\text{O}$ delivers a flux of neutrons allowing the s-process to take place. The efficiency of the s-process nucleosynthesis (in AGB stars with $M \leq 3 M_{\odot}$) depends on the abundances of the ^{13}C and ^{14}N in the ^{13}C pocket, on its extension in radius and mass, as well as on the rate of the nuclear reactions involved in the s-process and in the synthesis of the ^{13}C and the ^{14}N (see [4–6] and references therein). ^{14}N is produced in the ^{13}C -pocket by further proton captured on ^{13}C and it represents a poison of the s-process because of its large neutron capture cross section. Although it prevents the production of heavy elements, the ^{14}N is at the basis of another important nucleosynthesis network of AGB stars, the one that leads to the synthesis of ^{19}F via the $^{13}\text{C}(\text{p}, \gamma)^{14}\text{N}(\text{n}, \text{p})^{14}\text{C}(\alpha, \gamma)^{18}\text{O}(\text{p}, \alpha)^{15}\text{N}(\alpha, \gamma)^{19}\text{F}$ pathway. Notably, ^{19}F nucleosynthesis has been a matter of debate. Several astrophysical sites have been suggested for fluorine production (Type II supernovae [7], Wolf-Rayet stars [8–10], and merging white dwarf [11]), and among them, AGB stars are believed to be the main site of production of the stable isotope of fluorine in the Galaxy (see e.g., [12] and references therein). The interest in the ^{19}F abundance relies also on the possibility to probe different nucleosynthesis scenarios [13], since fluorine nucleosynthesis is extremely sensitive to the physical conditions inside stars.

Furthermore, nuclear production in AGB stars is important for the galactic chemical evolution of elements lighter than Fe, because of these stars capability to produce elements through the CNO, Ne-Na, and Mg-Al cycles. In this case, the H-capture reactions are responsible for the nucleosynthesis, however their coupling with mixing phenomena characterizes the yields. In stars more massive than $4\text{--}5 M_{\odot}$, the temperature at the base of the convective envelope is high enough (a few 10^7 K) to allow further proton captures to take place, and in lower mass AGB stars, non convective mixing mechanisms connect the H-burning layers directly with the stellar envelope, of which in both cases, stars show in their surface the same composition (or a composition similar to the one) of their inner and hotter layers where H is burning, e.g., high values of C/O, $^{12}\text{C}/^{13}\text{C}$, $^{14}\text{N}/^{15}\text{N}$, $^{16}\text{O}/^{18}\text{O}$, $^{26}\text{Al}/^{27}\text{Al}$.

For Hot Bottom Burning (HBB) [14], in more massive objects, as well as Cool Bottom Process (CBP) [15], in lower mass AGB stars, having high precision reaction rates is crucial to make accurate studies of proton capture nucleosynthesis in AGB stars. Indeed, isotopes such as ^7Li can undergo proton captures at few million Kelvin and the nucleosynthesis of other species, such as ^{17}O and ^{26}Al is sensitive to environmental temperature; therefore, their abundances can probe stellar interiors and/or, according to nuclear physics inputs employed in stellar models, might hit different scenarios for their production. For example, a current debate regard presolar oxide grains of group 2, indeed the abundances of oxygen isotopes measured in stellar dust can be accounted for in both their condensation in low mass AGB stars affected by CBP [16] as well as in more massive AGB stars affected by

HBB [17], the difference is made by the rates for the $^{17}\text{O}(p,\alpha)^{14}\text{N}$ and $^{17}\text{O}(p,\gamma)^{18}\text{F}$ reactions used in nucleosynthesis calculations [18].

This review is focused on the measurements of key reactions for AGB nucleosynthesis carried out by means of two indirect methods: the Trojan Horse Method (THM) [19–21] and the Asymptotic Normalization Coefficient (ANC) method [22–24].

2. Indirect Methods in Nuclear Astrophysics

Nuclear reaction cross section measurements of interest for nuclear astrophysics are difficult to be performed in terrestrial laboratories mainly because of Coulomb barrier penetration and electron screening effects [25]. In most of the cases, the Gamow energy region is explored via extrapolation procedures based on high-energy cross section measurements, thus possibly introducing systematic uncertainties as, for instance, those related to the presence of low-energy resonances, to the contribution of broad sub-threshold resonances or to the poor knowledge of the electron screening potential values [25]. In order to overcome these difficulties, indirect methods have been proved to be a valid complementary tool for experimental nuclear astrophysics since they allow the extraction of the astrophysically relevant cross section by selecting a precise reaction mechanism on a suitable reaction process thanks to devoted theoretical formalism [19]. In the next sections, the THM and ANC methods will be discussed in more detail.

2.1. The Trojan Horse Method

The Trojan Horse Method allows to obtain the two-body cross section at low energies:



from a suitable three-body reaction:



a , called the Trojan Horse nucleus, having a strong $x \oplus s$ cluster structure. Under appropriate kinematical conditions, it is possible to select the Quasi-Free (QF) contribution to the three-body break-up reaction where the particle A interacts only with the part x of the nucleus a , whereby the nucleus s can be considered as spectator during the reaction [26]. This direct reaction mechanism gives the dominating contribution to the cross section in a restricted region of the three body phase space when the momentum transferred to the spectator s is small, that is for QF scattering conditions. Since the energy and momentum of nucleus x do not obey the usual dispersion relation for a free particle, the transferred nucleus appears only as a virtual particle in the reaction process. If QF conditions are fulfilled, the spectator nucleus s is emitted with a momentum strictly connected to the momentum distribution of the cluster x inside a , the reaction mechanism being direct.

The QF reaction (1) can be described by a pole diagram with two vertices (see Figure 1): The upper pole describes the virtual break up of the nucleus a into the cluster x and s and the lower pole describes the binary reaction (1) that is relevant to astrophysics. This picture will be reflected in the expression relating the cross sections of the two reactions as a result of the theoretical description in certain approximations. By using the Plain Wave Impulse Approximation (PWIA), and denoting with $\mu_{ij} = m_i m_j / (m_i + m_j)$ and $\vec{p}_{ij} = \mu_{ij}(\vec{p}_i / m_i - \vec{p}_j / m_j)$, the reduced mass and the relative momenta of the two particles i and j , respectively, the three-body cross section (2) can be factorized in two terms corresponding to the break-up and to the reaction pole respectively [21]:

$$\frac{d\sigma_{A+a \rightarrow B+b+s}}{dE_{Bb} d\Omega_{Bb} d\Omega_{Fs}} = K |\tilde{\chi}_{xs}(\vec{Q}_{Fs})|^2 \frac{d\sigma_{A+x \rightarrow B+b}^{HOES}}{d\Omega_{Bb}}. \tag{3}$$

In Equation (3), $\tilde{\chi}_{xs}(\vec{Q}_{Fs})$ is the momentum space wave function in the center-of-mass system, being $\vec{Q}_{Fs} = \frac{m_s}{m_x + m_s} \vec{p}_a - \vec{p}_s$ (\vec{p}_a and \vec{p}_s are the momenta of the Trojan Horse nucleus

and of the spectator, respectively), $K = \frac{\mu_{Aa}\mu_{Fs}}{(2\pi\hbar)^3\mu_{Ax}} \frac{p_{Ax}p_{Fs}}{p_{Aa}} \frac{2J_x+1}{2J_a+1}$ is a kinematical factor where J_x and J_a represent the total angular momenta for the x and a nuclei and $\frac{d\sigma_{A+x \rightarrow B+b}^{HOES}}{d\Omega_{Bb}}$ is the half-off-shell cross section of the $A + x \rightarrow B + b$ reaction. Equation (3) shows the typical structure with three factors as a result of the PWIA: a kinematic factor, a momentum distribution, and a cross section of the two-body subprocess (1).

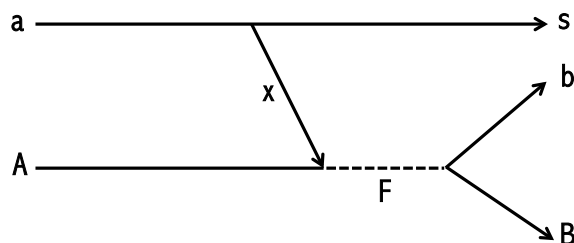


Figure 1. Scheme of a quasi-free Trojan Horse reaction $A(a,bB)s$. The upper vertex shows the $a \rightarrow x + s$ breakup. The lower vertex shows the reaction of astrophysical interest, which proceeds through the formation of intermediate system F . If the process is QF, the nucleus s will act as a spectator.

If the bombarding energy E_A is chosen high enough to overcome the Coulomb barrier in the entrance channel of the three-body reaction, both the Coulomb barrier and electron screening effects are negligible.

Nevertheless, the QF $A+x$ process can take place at sub-Coulomb, even negative, relative energy E_{Ax} , thanks to the key role of the $a = x \oplus s$ binding energy B_{sx} in compensating for the $A + a$ relative motion. In the QF kinematics $p_{sx} = 0$ and in the laboratory system (the target is at rest, which means $p_a = 0$ and $p_s = 0$), the so called “QF two body energy” is given by [27]:

$$E_{QF} = \frac{m_x}{m_x + m_A} E_A - B_{sx}. \tag{4}$$

This means that the binary reaction can be induced at very low E_{QF} in the THM using the beam energy E_A above the Coulomb barrier, a condition that is impossible to achieve in direct measurements due to the Coulomb barrier. It is important to notice that E_{QF} is uniquely determined from Equation (4) once the projectile energy is fixed.

For resonant cases, the TH double differential cross section can be written as [28–31]:

$$\frac{d^2\sigma^{TH}}{d\Omega_{\vec{p}_{sF}} dE_{bB}} = \frac{1}{2\pi} \frac{\Gamma_{bB}(E_{bB})}{(E_{bB} - E_{R_{bB}})^2 + \frac{1}{4}\Gamma^2(E_{bB})} \times \frac{d\sigma_{(A+a \rightarrow s+F)}}{d\Omega_{\vec{p}_{sF}}}, \tag{5}$$

where the differential $\frac{d\sigma_{(A+a \rightarrow s+F)}}{d\Omega_{\vec{p}_{sF}}}$ cross section has the form [31]:

$$\frac{d\sigma_{(A+a \rightarrow s+F)}}{d\Omega_{\vec{p}_{sF}}} = \frac{\mu_{sF} \mu_{Aa}}{4\pi^2} \frac{p_{sF}}{p_{Aa}} \frac{1}{J_A J_a} \times \sum_{M_F M_s M_A M_a} |M_{M_F M_s; M_A M_a}(\vec{p}_{sF}, \vec{p}_{Aa})|^2 \tag{6}$$

being J_i and M_i the spin of particle i and its projection, respectively. In PWIA, the transfer reaction amplitude M can be factorized as:

$$M_i \approx \phi(p_{xs}) W_{xA}^{F_i}(\vec{p}_{xA}), \tag{7}$$

where $\phi(p_{xs})$ is the Fourier transform of the radial $x - s$ bound-state wave function, p_{xs} is the $x - s$ relative momentum, while:

$$W_{xA}^{F_i}(\vec{p}_{xA}) = \langle I_{xA}^{F_i} | V_{xA} | \vec{p}_{xA} \rangle \quad (8)$$

is the form factor for the $A + x \rightarrow F_i$ process, leading to the feeding of the i -th excited state F_i . Therefore, Equation (5) represents an extension of Equation (3) to the case of resonant reactions and makes it possible to use more advanced approaches in the place of PWIA, such as DWBA or CDCC.

As stated above, THM is based on the theoretical formalism of the QF breakup extensively studied in the past. However, the PWIA formulations cannot coherently account for distortions and coupled-channel effects [21]. These limit the straight connection between the THM 2→3 reaction and the two-body reaction of astrophysical relevance and could cause the normalization constant (presently deduced by scaling to available direct data at high energies) to depend on the center-of-mass energy. To fulfill the PWIA prescription, we restrict the data analysis to only a small fraction of the available 2→3 body data, thus limiting the final available statistics, yet reducing systematic errors to value lower than the statistical one. Additionally, a key ingredient for THM applications is represented by the momentum distribution, connected with the intercluster motion inside the TH-nucleus. The study of the experimental momentum distribution is a very useful tool to size the effect of the aforementioned distortions. To date, only nuclei with a dominant s-wave intercluster motion are used for THM applications (such as ${}^2\text{H}$, ${}^3\text{He}$, ${}^6\text{Li}$, ${}^{14}\text{N}$) while further efforts are needed for adopting p-wave intercluster motion nuclei. For example, the role of momentum distribution and, in particular, of its derivation from the PWIA or DWBA approach has been discussed in [32,33] for the ${}^{18}\text{O}(p,\alpha){}^{15}\text{N}$ case. In the narrow spectator momentum range of 0–50 MeV/c, the difference between PWIA and DWBA momentum distributions is negligibly small, at a level of about 4%, thus hardly influencing the final THM cross section in the selected momentum window. Furthermore, in [34], the role of d-state component of the deuteron wave function was investigated, leading to variations at a level of about 1% as maximum, showing that the deduced cross sections are mildly dependent on the details of the momentum distribution. This is further demonstrated by the FWHM of the experimental momentum distribution in THM applications, which might be a function of the projectile energies under some condition, as discussed in [35]. In addition, in this case, the deduced cross sections hardly depend on the change in the width (which could be accounted for, anyway), since a variation of about 10% in the case of the ${}^6\text{Li}(d,\alpha)\alpha$ two body reaction is observed if no corrections are introduced. The influence of the shape of the momentum distribution was also investigated for the ${}^3\text{He}$ case [36], where a 3% difference was found between the experimental momentum distribution and the theoretical one. Furthermore, the shape analysis can also be used for discerning if reaction mechanisms, other than the QF ones, affect THM data. For instance, the analysis made in [37] leads to a negligible contribution ($\sim 3\%$) on the final reaction rate evaluation.

The method has been largely tested and applied to shed light on different issues, ranging from pure nuclear physics (as the p + p proton scattering [38] or clusterization effects and the relative impact for electron screening [39,40]) to various contexts in nuclear astrophysics (as primordial nucleosynthesis [41,42], lithium problem [43,44] and light elements depletion [45–48], AGB and Novae nucleosynthesis [49], and carbon burning [37]). Recently, the method has been extended to the indirect study of neutron-induced reactions [50,51] and to reactions of astrophysical interest induced by radioactive ion beams [52,53], opening a new field of research, overcoming all the experimental difficulties related to the direct measurements of neutron-induced reactions with unstable beams [54,55].

2.2. The Asymptotic Normalization Coefficient

The Asymptotic normalization coefficients method consists in retrieving the cross section for a $A(a,\gamma)B$ reaction from a suitable $A(X,Y)B$ one, in which $X = Y + a$ and $B = A + a$. Such a method has been used proficiently to investigate low energy proton [56], neutron [57],

and α [58] captures of astrophysical interest. More recently an extension of the method has also been developed for mirror nuclei [59], with the aim to study proton or neutron capture from the analysis of a suitable mirror reaction [60–62].

For one-particle transfer reactions, the differential cross section for the $A + a \rightarrow Y + B$ reaction (Figure 2) can be parameterized, using Distorted Wave Born Approximation (DWBA) as:

$$\frac{d\sigma}{d\Omega} = \sum_{j_B, j_X} S_{Aa, l_B, j_B} S_{Ya, l_X, j_X} \sigma_{l_B, j_B, l_X, j_X}^{DWBA} \tag{9}$$

S_{Aa, l_B, j_B} and S_{Ya, l_X, j_X} being the so called *spectroscopic factors* for the initial and final state associated to a specific bound state. Focusing on the $A + a \rightarrow B$ vertex of Figure 2, the radial overlap function I_{Aa, l_B, j_B}^B can be approximated by the wave function of the bound state ($B = A + a$) [63]:

$$I_{Aa, l_B, j_B}^B(r_{Aa}) = S_{Aa, l_B, j_B}^{1/2} \phi_{Aa, l_B, j_B}(r_{Aa}). \tag{10}$$

In Equation (10), the spectroscopic factor S_{Aa, l_B, j_B} is related to the $A+a$ configuration with quantum number l_B and j_B , while $\phi_{Aa, l_B, j_B}(r_{Aa})$ represents the bound state wave-function of the $A + a$ system.

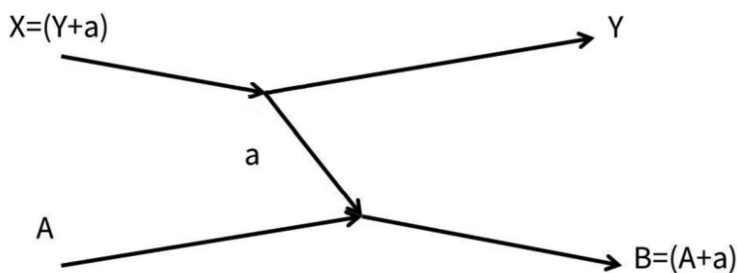


Figure 2. Sketch of a typical transfer reaction used to measure the ANC: The transferred particle a can usually be a proton, a neutron or a α -particle.

In case of a peripheral reaction (such as the transfer ones at low energies), both the radial overlap integral and bound state wave function can be written in their asymptotic limit in terms of the Whittaker function $W_{-\eta, l_{Aa}+1/2}$, where η is the Sommerfeld parameter:

$$I_{Aa, l_B, j_B}^B \xrightarrow{r_{Aa} > R_n} C_{Aa, l_B, j_B}^B \frac{W_{-\eta, l_{Aa}+1/2}(2k_{Aa} r_{Aa})}{r_{Aa}} \tag{11}$$

$$\phi_{Aa, l_B, j_B}^B \xrightarrow{r_{Aa} > R_n} b_{Aa, l_B, j_B}^B \frac{W_{-\eta, l_{Aa}+1/2}(2k_{Aa} r_{Aa})}{r_{Aa}}. \tag{12}$$

In both Equations (11) and (12), the Whittaker function depends on the interaction radius (r_{Aa}) and on the wave number $k_{Aa} = \sqrt{\frac{2\mu_{Aa}\epsilon_a}{\hbar^2}}$, with μ_{Aa} as the reduced mass of the $A + a$ system and ϵ_a as the separation energy of the a particle from the B nucleus. The coefficients C_{Aa, l_B, j_B}^B and b_{Aa, l_B, j_B}^B are the so-called ANC and *single-particle ANC* (or SPANC), the latter representing the normalization coefficient of the radial single-particle bound-state wave-function tail. This quantity is strongly connected to the single-particle potential used to reproduce the bound states of the $B = A + a$ system. Using Equations (11) and (12) in Equation (10), we obtain that the spectroscopic factor S can be written in terms of ANC and SPANC:

$$S_{Aa, l_B, j_B}^2 = \frac{\left(C_{Aa, l_B, j_B}^B\right)^2}{\left(b_{Aa, l_B, j_B}^B\right)^2}. \tag{13}$$

Using the same procedure for the $X = Y + A$ vertex of Figure 2, the differential cross section (Equation (9)) can be finally written as:

$$\frac{d\sigma}{d\Omega} = \sum_{j_B, j_X} \left(C_{Aa, l_B, j_B}^B \right)^2 \left(C_{Ya, l_X, j_X}^X \right)^2 \frac{\sigma_{l_B, j_B, l_X, j_X}^{DWBA}}{b_{Aa, l_B, j_B}^2 b_{Ya, l_X, j_X}^2}. \quad (14)$$

The advantage of this procedure lies in the fact that, with respect to the spectroscopic factor, for peripheral reactions, the ANC is weakly dependent from the adopted potential [64–67]. Indeed, by properly selecting the kinematical conditions ensuring the peripheral character of the transfer reaction, the uncertainties related to the ANC calculations are mainly related to the well-known model dependence of DWBA calculations due, for instance, to the choice of the OMP and to the transferred single particle wave function. Usually, these uncertainties are estimated to be at most 15% for the OMP and at most 10% for the bound-state particle wave function (see [62,63,68] for example). These uncertainties, together with the experimental ones (i.e., statistical error, target thickness evaluation, background evaluation, and evaluation of the solid angle) return a final error budget that, depending on the physics case, can be as low as 5% as in the recent ${}^3\text{He}(\alpha, \gamma){}^7\text{Be}$ and ${}^6\text{Li}(p, \gamma){}^7\text{Be}$ ANC investigations [58,69]. This uncertainty value can be achieved by a careful selection of the transfer process and by constraining the OMP by fitting the elastic scattering cross sections for the entrance and exit channel particles [58,69].

A more extended review of the method, along with a collection of remarkable results useful for astrophysics can be found in [70].

3. The ${}^{17,18}\text{O}(p, \alpha){}^{14,15}\text{N}$ and ${}^{17,18}\text{O}(p, \gamma){}^{18,19}\text{F}$ Reactions

In Red Giant Branch (RGB) and AGB stars, the relevant temperatures for the ${}^{17}\text{O}$ and ${}^{18}\text{O}$ nucleosynthesis are in the ranges $T_9 = 0.01\text{--}0.1$ ($T_9 = T/10^9$ K), corresponding to an center-of-mass energy window ranging from ~ 20 up to ~ 150 keV. Thus, the cross sections of the ${}^{18}\text{O}(p, \alpha){}^{15}\text{N}$, ${}^{17}\text{O}(p, \alpha){}^{14}\text{N}$, ${}^{17}\text{O}(p, \gamma){}^{18}\text{F}$, and ${}^{18}\text{O}(p, \gamma){}^{19}\text{F}$ reactions have to be precisely known in the center-of-mass energy lower than $E_{c.m.} = 100$ keV. At these energies resonance reactions play a decisive role because the astrophysical $S(E)$ -factor, a function proportional to the cross section that contains all the strictly nuclear effect [25], might be dramatically enhanced by the presence of a resonance, whose measurement is then crucial to pin down the astrophysical scenario [71].

The ${}^{17}\text{O}(p, \alpha){}^{14}\text{N}$ reaction is dominated, in the energy region of our interest, by two resonances at about 65 keV and 183 keV above the ${}^{18}\text{F}$ proton threshold. The $E_{c.m.} = 65$ keV resonance has been measured by applying the THM to the quasi-free ${}^2\text{H}({}^{17}\text{O}, {}^{14}\text{N}\alpha)n$ reaction and by normalizing experimental data to the weighted average of the four values for the 183 keV resonance strength reported in the literature [72–75]. The study of the ${}^{17}\text{O}(p, \alpha){}^{14}\text{N}$ via the THM application was carried out in two experiments: The first one at the Laboratori Nazionali del Sud (LNS) in Catania (Italy) and the second one at the Institute for Structure and Nuclear Astrophysics (ISNAP) of the University of Notre Dame (USA). In the LNS experiment, the SMP Tandem Van de Graaff accelerator provided a 41-MeV ${}^{17}\text{O}$ beam impinging on a deuterated polyethylene target (CD_2) of about $150 \mu\text{g}/\text{cm}^2$ placed at 90° with respect to the beam axis. In the NSL experiment, a beam energy of 43.5 MeV and a target thickness of $170 \mu\text{g}/\text{cm}^2$ were used. The experimental setup and the data analysis of the LNS and at NSL experiments are extensively discussed in [76,77]. The main result of these two experimental studies is the 65-keV resonance strengths obtained in the LNS experiment, $((\omega\gamma)_{LNS}^{THM} = (3.72 \pm 0.78) \times 10^{-9}$ eV) and in the NSL experiment, $((\omega\gamma)_{NSL}^{THM} = (3.16 \pm 0.68) \times 10^{-9}$ eV). The adopted value $((\omega\gamma)_{p, \alpha}^{THM} = (3.42 \pm 0.60) \times 10^{-9}$ eV), obtained as a weighted average between the two strengths, was used to calculate the contribution of the 65 keV resonance to the total reaction rate adopting the narrow resonance approximation, whose conditions are satisfied for the resonance under investigation [73].

Panel (a) of Figure 3 shows the ratio (blue middle line) between the THM reaction rate and the reaction rate reported in [73] (see [77] for more details). The other blue lines in

Figure 3a mark the positions of the high and low rates as deduced in [77]. The black dotted area represents the range of variation for the reaction rate of [73]. A significant variation ($\sim 30\%$) can be seen in the range $T_9 = 0.02\text{--}0.07$, while no significant differences are present for higher temperatures.

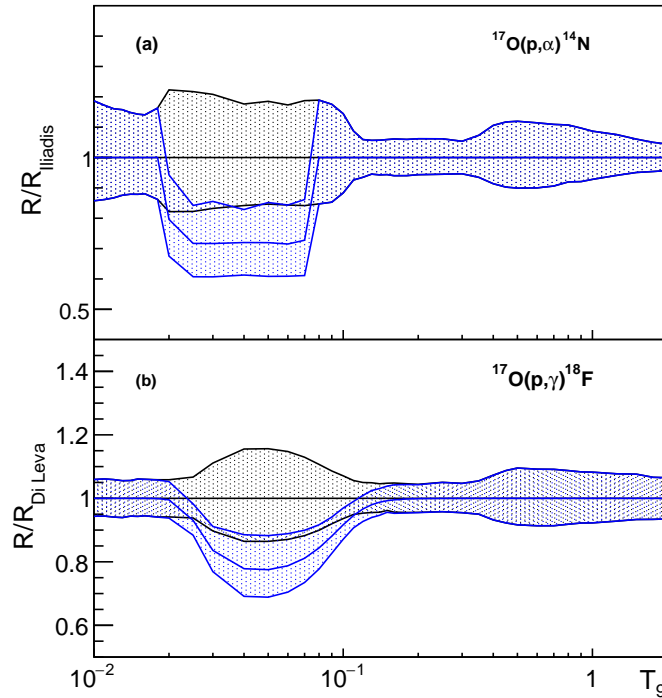


Figure 3. (a) Comparison of the THM reaction rate (blue lines) of the $^{17}\text{O}(p,\alpha)^{14}\text{N}$ reaction with the direct one [73] (black lines). (b) Comparison of the THM reaction rate (blue lines) of the $^{17}\text{O}(p,\gamma)^{18}\text{F}$ reaction with the direct one [78] (black lines).

In 2016, a new direct measurement [79] of the 65-keV resonance strength performed at the Laboratory for Underground Nuclear Astrophysics (LUNA) accelerator has led to a value $\omega\gamma = 10.0 \pm 1.4_{\text{stat}} \pm 0.7_{\text{syst}}$ neV, a factor of 3 larger with respect to the value obtained by using the THM [77].

Since the strengths of the $E = 65$ keV resonance in both (p,α) and (p,γ) channels are proportional to the proton partial width Γ_p and the exit channel partial width essentially coinciding with the total width through the statistical factor, by using the formula:

$$(\omega\gamma)_{p\gamma}^{\text{THM}} = (\omega\gamma)_{p\alpha}^{\text{THM}} \frac{\Gamma_\gamma}{\Gamma_\alpha} \tag{15}$$

the 65-keV resonance strength in the (p,γ) channel can be evaluated, obtaining the value $(\omega\gamma)_{p\gamma}^{\text{THM}} = (1.18 \pm 0.21) \times 10^{-11}$ eV. This value is 39% smaller than the value of $(1.6 \pm 0.3) \times 10^{-11}$ eV given in the literature [72,80] and in the most recent reviews ([73,81], 2011). The Γ_γ and Γ_α values used in Equation (15) are those reported in [73]. Panel (b) of Figure 3 shows the ratio (blue middle line) of the THM reaction rate to reaction rate evaluation R_{DiLeva} reported in [78] (black line) for the $^{17}\text{O}(p,\gamma)^{18}\text{F}$ reaction. The blue dotted area marks the reaction-rate interval allowed by the experimental uncertainties on the 65-keV resonance strength only, while the black dotted area is used to display the uncertainty range characterizing direct data [78]. In addition, for this case, a significant reduction ($\sim 20\%$) of the reaction rate in the $T_9 = 0.03\text{--}0.09$ temperature range was obtained due to the THM measurement of the 65-keV resonance strength. A possible explanation for the discrepancies between direct and THM results in both (p,α) and (p,γ) channels could be

attributable to the electron screening effect that was not taken into account in the direct measurements (see [77] for more details).

At temperatures typical of H-burning in AGB stars, the energy interval where the $^{18}\text{O}(p,\alpha)^{15}\text{N}$ is most effective ranges from about 20 to 70 keV. In this energy range only, the 20, 144, and the broad 656 keV resonances are relevant for astrophysics as they determine the reaction rate [82]. Since the strength of the 20 keV resonance was known only from spectroscopic measurements [83] and from the direct capture reaction $^{18}\text{O}(p,\gamma)^{19}\text{F}$ [84], the narrow-resonance formalism of THM was employed to obtain its strength [30,85]. In particular, the cross section of the $^{18}\text{O}(p,\alpha)^{15}\text{N}$ reaction was deduced by applying the THM to the $^2\text{H}(^{18}\text{O},\alpha)^{15}\text{N}n$ three-body process, performed in QF kinematics. The experiment was performed at Laboratori Nazionali del Sud, Catania (Italy). The SMP Tandem Van de Graaf accelerator provided the 54 MeV ^{18}O beam, which was accurately collimated to minimize angular straggling (about 0.06°) [32]. A description of the data analysis is reported in [32]; here we discuss only the main results. In particular, the strength of the 20 keV resonance was obtained by normalizing the TH data to the well-known resonance at 144 keV [86]. The TH strength results in $\omega\gamma = (8.3_{-2.6}^{+3.8}) \times 10^{-19}$ eV, which is in good agreement with $\omega\gamma = (6_{-5}^{+17}) \times 10^{-19}$ eV, reported by [82] but 10 times more accurate. The comparison between the obtained reaction rate and the one reported in Nuclear Astrophysics Compilation of REaction rates (NACRE) [82] is given in Figure 4. In this representation, the ratio of the THM reaction rate to the NACRE one is given by a full blue line while the NACRE rate is given by a full black line. The blue dotted area marks the reaction-rate interval allowed by the THM experimental uncertainties, while the black dotted area is used to display the uncertainty range characterizing direct data [82]. Clearly, the THM reaction rate shows a much narrower band than the direct one [82] over the whole temperature range, especially at low temperatures, $T_9 < 0.03$, thanks to the enhanced precision of the strength of the 20-keV resonance measured by the THM.

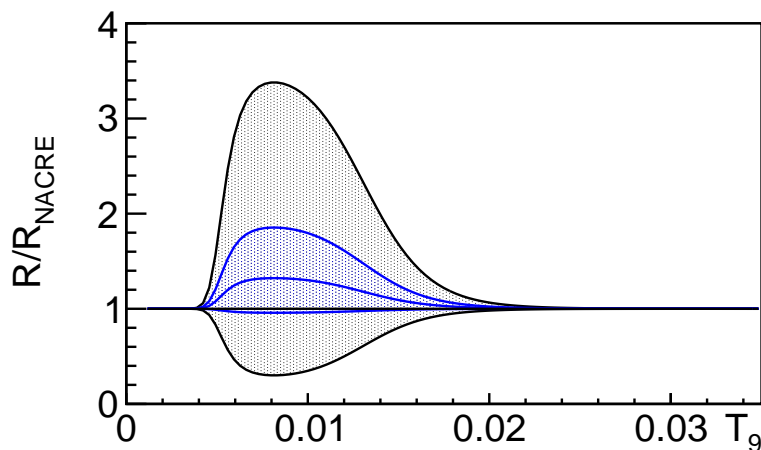


Figure 4. Comparison of the THM reaction rate (black lines) of the $^{18}\text{O}(p,\alpha)^{15}\text{N}$ reaction with the NACRE one [82] (blue lines). The full lines are the ratio of the recommended rate to the NACRE one. The blue dotted area marks the reaction-rate interval allowed by the THM experimental uncertainties, while the black dotted area is used to display the uncertainty range characterizing direct data [82].

The effect of the recent THM measurement of the $^{17}\text{O}(p,\alpha)^{14}\text{N}$, $^{18}\text{O}(p,\alpha)^{15}\text{N}$ and $^{17}\text{O}(p,\gamma)^{18}\text{F}$ low energy cross sections has been investigated on nitrogen and oxygen isotopic abundances in RGB and AGB stars [71]. In fact, the CNO isotope supply is very sensitive to the extra-mixing phenomena, significantly altering their surface abundance and strong constraints can be set on models using the observed isotopic ratios in circumstellar condensates found in meteorites. Assuming the extra-mixing model, as widely discussed in [71], the coupled CNO nucleosynthesis was followed, alternatively introducing into the post-processing codes the THM reaction rates and the ones in the literature [72,81,82].

The change in the $^{18}\text{O}(p,\alpha)^{15}\text{N}$ reaction rate stemming from the revised 20-keV resonance strength does not significantly influence either ^{15}N or ^{18}O abundances, ^{18}O being easily destroyed by proton-capture reactions. For this reason, the introduction of this newly measured cross section into extramixing calculations confirms that the low $^{14}\text{N}/^{15}\text{N}$ isotopic ratios found in A + B and Mainstream SiC grains have no nuclear reaction origin related to the $^{18}\text{O}(p,\alpha)^{15}\text{N}$ channel. Conversely, the reduced efficiency of proton captures on the ^{17}O nuclei given by the new THM reaction rates show an increase of the $^{17}\text{O}/^{16}\text{O}$ equilibrium values by about 30% with respect to the literature. This leads to a better agreement between predicted $^{17}\text{O}/^{16}\text{O}$ isotopic ratios and experimental values retrieved from group 2 oxide grains, which are characterized by an excess of ^{17}O and a large ^{18}O depletion with respect to the solar values. Therefore, extra-mixing calculations performed with the TH reaction rates strengthen the idea that those grains were formed in the envelope of low-mass AGB stars (for more details, see [71] and reference therein).

Even if the $^{18}\text{O}(p,\alpha)^{15}\text{N}$ reaction is the dominant ^{18}O destruction channel via proton capture in an AGB environment [85,87], the competing $^{18}\text{O}(p,\gamma)^{19}\text{F}$, whose rate is about three orders of magnitude lower at solar energies, represents the main reaction channel to escape the cycle, with the direct part of the (p,γ) process representing the main contributor to the reaction at astrophysical energies.

The $^{18}\text{O}(p,\gamma)^{19}\text{F}$ reaction has been largely investigated in the past: the direct component of the excitation function has been determined experimentally and theoretically by [84], confirming the contribution of three low-energy resonances as in [88,89]. On the other hand, some discrepancies were found by [90] concerning the behavior of the $^{18}\text{O}(p,\gamma)^{19}\text{F}$ direct component at low energies that shows an increasing trend with energy instead of the decreasing one obtained by [84]. For this reason, the $^{18}\text{O}(p,\gamma)^{19}\text{F}$ reaction was investigated again by means of the ANC method [56]. The radiative capture cross section for the reaction $^{18}\text{O}(p,\gamma)^{19}\text{F}$ was retrieved from the $^{18}\text{O}(^3\text{He},d)^{19}\text{F}$ one, using the 24.6 MeV ^3He beam provided by the U-120M iso-chronous cyclotron of the Nuclear Physics Institute of the Czech Academy of Sciences. The gas target chamber, filled with 99% purity ^{18}O gas, was made to have an output window that covers an angular range from -65° to $+40^\circ$, allowing the detection of particles in the angular range of interest. Eight ΔE -E telescopes, of a different thickness as reported in [56] were used to identify and detect the outgoing particles, the ones of interest being the scattered ^3He and the deuterons from the transfer reaction.

The optical model parameters (OMP's) for the input channel were deduced from the elastically scattered ^3He particles off ^{18}O . Such OMP's turned out to be the same of [91] and [92]. In this experiment, 11 peaks belonging to the deuterons coming from the reaction $^{18}\text{O}(^3\text{He},d)^{19}\text{F}$ were identified: such particles correspond to the transitions to the bound state of ^{19}F nucleus (an example can be found in Figure 5). The OMP's for the outgoing channel were taken from the global formula of [93] at the proper energy and used to reproduce the extracted deuteron angular distributions.

Once the OMP's for the entrance channel and for the exit ones (captured in the ground state and in 12 excited states) are properly set, using Equation (14) it was possible to calculate the ANC's for the detected states (see Table 3 in [56]), using three different interaction potentials for the $^{19}\text{F} \rightarrow p + ^{18}\text{O}$ system: To do so, the authors used the value of $C_{dp}^2/b_{dp}^2 = 1.31$ taken from [94] for the system $^3\text{He} \rightarrow d + p$. In two of the three cases analyzed, the resulting astrophysical S-factor shows a trend that is similar to [90], however the direct contribution is lower than in both [84,90]. This discrepancy is due to the fact that the ANC method covers just the direct part of the total S-factor (Figure 6).

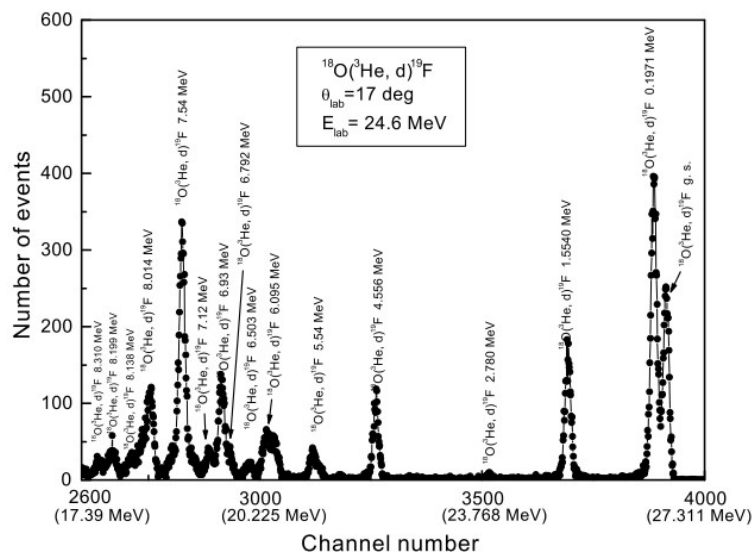


Figure 5. Part of the spectrum of deuterons from the reaction $^{18}\text{O}(^3\text{He},d)^{19}\text{F}$ at $\theta_{lab} = 17^\circ$ as reported in [56].

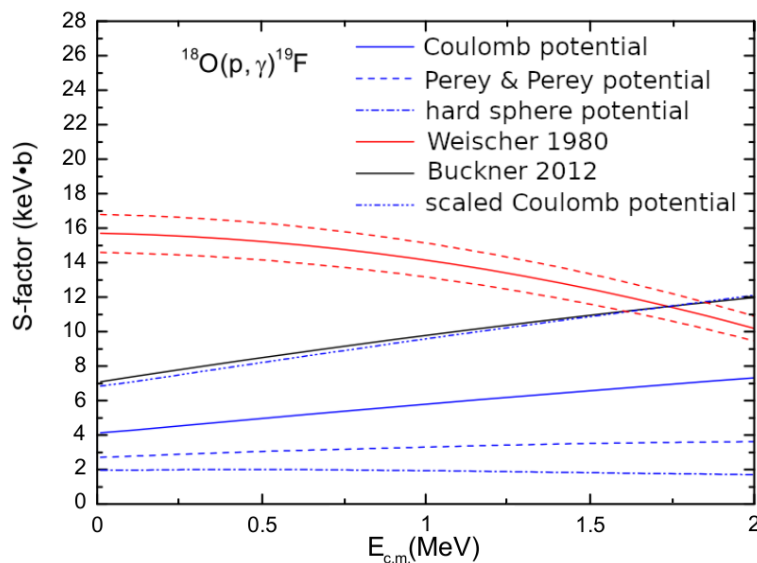


Figure 6. S-factor of the total direct proton capture $^{18}\text{O}(p,\gamma)^{19}\text{F}$ determined using ANC (picture taken from [56]): The dashed blue line obtained using the Perey and Perey potential [93] shows an opposite trend with respect to [84] (red solid line). The $S(E)$ -factor extracted by [90] (solid black line), along with calculation performed using Coulomb (solid blue line) and hard sphere potentials (dashed-dotted blue lines). A Coulomb potential scaled on data from the results of [90] is also reported.

4. The $^{15}\text{N}(p,\alpha)^{12}\text{C}$ Reaction

Concerning the ^{15}N isotope in AGB stars nucleosynthesis, it takes a key role in the ^{19}F production via the $^{15}\text{N}(\alpha,\gamma)^{19}\text{F}$ reaction. Thus, proper knowledge of the competing $^{15}\text{N}(p,\alpha)^{12}\text{C}$ reaction is of primary importance since it reduces the amount of both proton and ^{15}N nuclei available for the ^{19}F production [95]. The $^{15}\text{N}+p$ interaction takes place at typical temperatures of about $T_9 = \sim 10^{-2} - 10^{-1}$, corresponding to a Gamow energy window ranging from ~ 20 keV up to ~ 200 keV. The NACRE reaction rate was obtained by interpolating the experimental data discussed in [96–98] and by evaluating the contribution of high-energy resonances (see [82] for a detailed discussion). In particular, the $^{15}\text{N}(p,\alpha)^{12}\text{C}$ cross section measurement of [98] spans the energy range $E_{c.m.} \sim 73\text{--}759$ keV, thus partially

covering the Gamow energy window. The extrapolated zero-energy astrophysical factor $S(0) = 65 \pm 7$ MeV b was obtained from the Breit–Wigner extrapolation [98].

In order to explore the whole Gamow energy window, a devoted $^{15}\text{N}(p,\alpha)^{12}\text{C}$ THM measurement was performed by selecting the QF contribution of the $^2\text{H}(^{15}\text{N},\alpha)^{12}\text{C}$ three-body reaction, by using the deuteron as the TH nucleus [99]. The experiment was performed at the Texas A&M University Cyclotron Institute delivering a 60 MeV ^{15}N beam onto a $150 \mu\text{g}/\text{cm}^2$ CD_2 target. More details on the experimental setup and on the data analysis procedure can be found in [99].

The THM investigation allowed to extract the $S(E)$ -factor in the energy range $E_{c.m.} = 19$ –576 keV by normalizing the THM data to the direct ones by equating the areas under the 312 keV resonant peak due to the 12.44 MeV ^{16}O level ($\Gamma = 91$ keV, $J^\pi = 1^-$) [99]. In order to obtain the $S(E)$ -factor for zero relative energy, THM data were fitted taking into account the sum of a second-order polynomial and a Breit–Wigner function. In Figure 7, the THM $S(E)$ -factor (full red dots) of [99] is shown together with the result of the fitting procedure (red line) and the direct data of [96–98] (open circles, open squares, and open triangles, respectively). The black line represents the Breit–Wigner parametrization discussed in [98]. The THM measurement leads to the value of $S(0) = 62 \pm 10$ MeV b, in good agreement with previous estimations from direct measurements [96–98]. The uncertainty on the THM $S(0)$ value includes statistical, normalization, and extrapolation errors (see [99] for details).

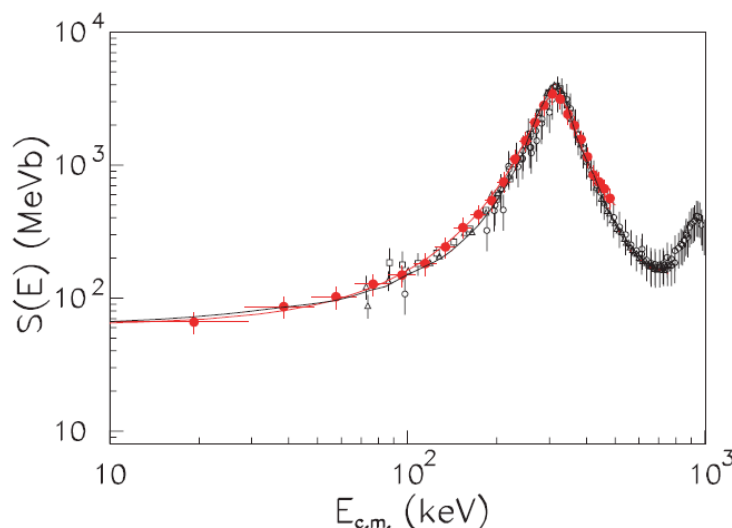


Figure 7. THM $S(E)$ -factor is shown as full red dots. The direct data from [96–98] are also shown as open symbols (circles, squares, and triangles, respectively). The red line represents a fit to the THM data. The black line is the result of the Breit–Wigner parametrization reported in [98].

A new paper by La Cognata et al. [31] provided an improved R-matrix fit of the $^{15}\text{N}(p,\alpha)^{12}\text{C}$ $S(E)$ -factor, taking into account both direct data and indirect Trojan Horse data. Authors obtained a more accurate recommended value for the zero-energy astrophysical factor. In particular, the new fit gave a $S(0) = 73.0 \pm 5.0$ MeV b from direct [98] and $S(0) = 70.0 \pm 13.5$ MeV b from the Trojan Horse data [99].

5. The Fluorine Problem: Study of the $^{19}\text{F}(p,\alpha_0)^{16}\text{O}$ and $^{19}\text{F}(\alpha,p)^{22}\text{Ne}$ Reactions

The $^{19}\text{F}(p,\alpha)^{16}\text{O}$ nuclear reaction represents the dominant channel for the fluorine burning in the H-burning shell of AGB stars. Indeed, the extramixing phenomena can expose the stellar material to temperatures large enough to activate the $^{19}\text{F}(p,\alpha)^{16}\text{O}$ reaction [13,76,100], thus depleting the fluorine surface abundance [13]. For a better understanding and for properly modeling these phenomena, the role of the $^{19}\text{F}(p,\alpha)^{16}\text{O}$ reaction has to be evaluated at energies of $E_{c.m.} \sim 30$ –300 keV, with the $^{19}\text{F}(p,\alpha_0)^{16}\text{O}$ channel being the dominant one at energies of $E_{c.m.} \lesssim 300$ keV [101].

The direct measurements included in the NACRE compilation [82] provided the $^{19}\text{F}(p,\alpha_0)^{16}\text{O}$ S(E)-factor down to about 460 keV [102], well above the energy range of astrophysical interest. Consequently, the adopted reaction rate was obtained by extrapolating the low-energy S(E)-factor via non-resonant behavior [82].

In 2015, the measurement of [103] allowed for deriving the S(E)-factor in the energy range $E_{c.m.} \sim 0.2\text{--}0.6$ MeV, confirming the contribution of ^{20}Ne excited levels at energies lower than ~ 600 keV's, as suggested also in [104]. Recently, the γ -ray yields were measured over $E_{c.m.} = 72.4\text{--}344$ keV, covering the Gamow window [105]. The experiment was performed under the extremely low cosmic-ray-induced background environment of the China JinPing Underground Laboratory and the obtained S(E) factors deviate significantly from previous theoretical predictions, and the uncertainties are significantly reduced.

In order to cover the full energy range of astrophysical interest, two devoted $^{19}\text{F}(p,\alpha_0)^{16}\text{O}$ THM experiments were performed¹ [104,108,109].

The first measurement was performed at LNS-INFN where the THM was applied to the $^2\text{H}(^{19}\text{F},\alpha^{16}\text{O})\text{n}$ three-body reaction. A 50 MeV ^{19}F beam was delivered onto a CD_2 target, where the deuteron was chosen as the “TH-nucleus” because its obvious p-n structure, its low-binding energy (B.E. = 2.22 MeV), and well-known momentum distribution for the p-n relative motion mostly occurring in s-wave [34]. More details on the experimental setup and on the data analysis, performed via the Modified R-Matrix formalism [32], can be found in [104].

The THM approach allowed to derive the S(E)-factor from 1 MeV down to zero energies and to further investigate, for the first time, the contribution of three different resonances at $E_{c.m.} = 113$ keV, 204 keV, and 382 keV due to the population of the ^{20}Ne excited states (see [104] for further details). Then, the $^{19}\text{F}(p,\alpha_0)^{16}\text{O}$ reaction rate was evaluated and compared with the NACRE one. The contribution of the 113 keV resonance leads to a large increase of the THM reaction rate with respect to the non-resonant one evaluated in the NACRE compilation, with a maximum difference of about 70% at $T_9 \approx 0.1$ [104]. The other resonant structures observed below 450 keV give a small contribution to the total reaction rate [104]. Additionally, thanks to the recent direct measurements of [110], a further reanalysis of the available $^{19}\text{F}(p,\alpha_0)^{16}\text{O}$ THM data was performed in [108]. The obtained results showed how the new normalization negligibly alters the results of [104].

Due to the low-energy resolution affecting the THM data of [104], it was not possible to retrieve definitive information on the contribution of the 204-keV and 251-keV resonances intervening in the $^{19}\text{F}(p,\alpha_0)^{16}\text{O}$ excitation function.

For such a reason, a second THM investigation of the $^{19}\text{F}(p,\alpha_0)^{16}\text{O}$ reaction was carried out via the study of the quasi-free $^2\text{H}(^{19}\text{F},\alpha^{16}\text{O})\text{n}$ reaction performed at the INFN national laboratories of Legnaro (LNL-INFN) [109].

Due to the improved energy resolution, the contribution of the 251-keV resonance was properly taken into account for the evaluation of the updated THM reaction rate. The ratio between the THM reaction rate and the NACRE one is shown in Figure 8 [109]. In the temperature range $0.04 \lesssim T_9 \lesssim 0.4$, the THM reaction rate significantly deviates from the NACRE one up to a factor of ~ 2 at about $T_9 \approx 0.1$. Although the updated reaction rate of [109] is in agreement with the previous THM one of [108], it deviates of $\sim 30\%$ at temperatures $T_9 \approx 0.4$ because of the constructive interference between the 113 and 251 keV resonances properly evaluated thanks to the improved THM experiment, as discussed in detail in [109].

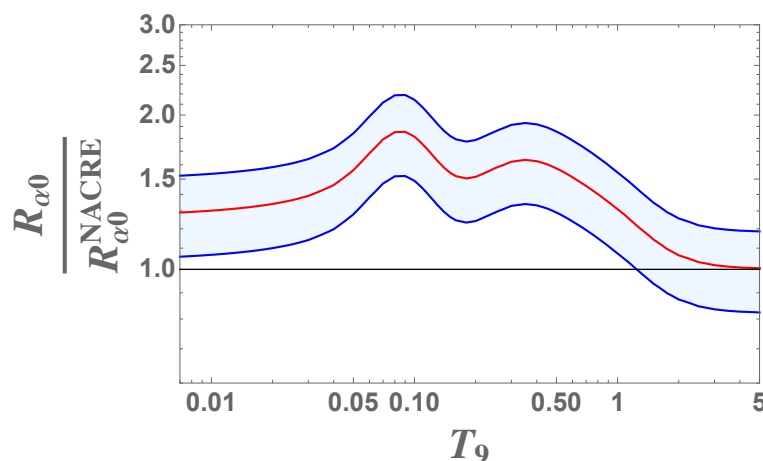


Figure 8. Ratio between the $^{19}\text{F}(p,\alpha_0)^{16}\text{O}$ THM reaction rate [109] and the NACRE recommended one [82] (red line). The estimated uncertainties on THM data are reported as a blue band. The black line corresponds to a ratio equal to 1.

The impact of the THM reaction rates [108,109] on the fluorine nucleosynthesis in AGB stars was then evaluated in [111]. As expected, the models adopting the THM reaction rates return lower fluorine abundances with respect to the calculations employing the NACRE reaction rate [82]. However, despite the adopted $^{19}\text{F}(p,\alpha_0)^{16}\text{O}$ THM reaction rates, the results of the theoretical models poorly differ if compared with the present observational uncertainties thus suggesting the need for more accurate stellar observations in order to better understand extra-mixing phenomena in AGB stars [111].

Besides the role played by the proton-induced reactions occurring in the H-shell, alpha-induced processes need also to be studied since they can be triggered in the He-shell of AGB stars and influence the final abundance of ^{19}F . In these scenario, an important role is played by $^{19}\text{F}(\alpha, p)^{22}\text{Ne}$ reaction, as suggested by [95,112].

The $^{19}\text{F}(\alpha, p)^{22}\text{Ne}$ reaction rate was affected by large uncertainties in correspondence of the He-burning temperatures ($0.4 \leq T_9 \leq 0.9$), due to the lack of low-energies experimental data. Indeed, the cross section measurements of [113] stop at energies of about $E_{c.m.} = 660$ keV, thus only partially covering the astrophysical relevant energy region (i.e., $\approx 0.2\text{--}1$ MeV).

For this reason, the $^{19}\text{F}(\alpha, p)^{22}\text{Ne}$ was studied by means of THM [114,115]. The measurement was carried out at the Ruđer Bošković Institute (Zagreb – HR), using the available 6 MeV ^6Li beam to trigger the quasi-free $^{19}\text{F}(^6\text{Li}, p)^{22}\text{Ne}d$ reaction, by using the ^6Li as “TH-nucleus”. After the selection of the quasi-free process, the angular distributions of the $^{19}\text{F}(\alpha, p)^{22}\text{Ne}$ reaction were deduced in correspondence to the energy range relevant for astrophysics, i.e., $0 \leq E_{c.m.} \leq 0.9$ MeV. The analysis performed in [114,115] underlined the predominance of the $l = 2$ contribution ($J^\pi = 3/2^+, 5/2^+$) for the 11 identified resonances, in agreement with the spin-parity and angular momentum assignment made by [113] for higher energies. To derive the astrophysical $S(E)$ -factor, a weighted fit of the cross section was performed by means of the one-level, three-channel *Modified R-Matrix* approach [114]. The $^{19}\text{F}(\alpha, p)^{22}\text{Ne}$ reaction rate was then calculated and compared with the one of [113], resulting in an increase of up to a factor ~ 4 (considering the upper limit) in the temperature range of interest, as shown in Figure 9 [114,115].

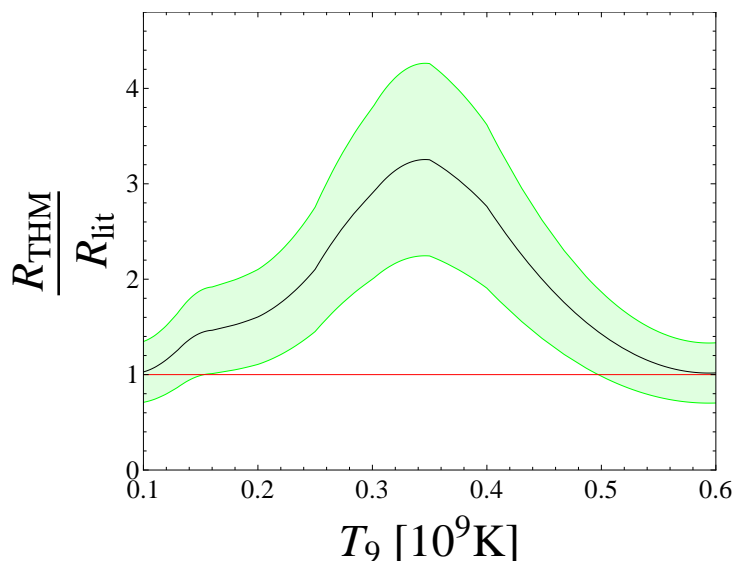


Figure 9. Ratio of the $^{19}\text{F}(\alpha, p)^{22}\text{Ne}$ THM reaction rate to the one calculated in [113] (R_{lit}). The estimated uncertainties of the THM data are reported as a green band (see [114] for details).

The THM reaction rate was then used to evaluate the impact on the nucleosynthesis of low-mass AGB stars using the *NEWTON* [116] code for three stellar models of 1.5, 3, and 5 M_{\odot} with solar metallicity, and ^{19}F destruction revealed to be more efficient in the AGB environment of up to a factor of 5. Nonetheless, the temporal evolution of fluorine abundance in this context shows a variation that is smaller than 5% with respect to the calculation performed using the rate from [113] in the stellar envelope.

6. Neutron Sources for s-Processes: The $^{13}\text{C}(\alpha, n)^{16}\text{O}$ Reaction

The key ingredient for activating the s-process reactions in stellar environments is a neutron source [117].

For this reason, several candidate reactions were proposed over the years [118]. However, in a stellar interior, identifying the neutron reaction with the highest rate is not the only relevant parameter in predicting the main source of neutrons for s-process nucleosynthesis [2]. Our current understanding of s-process nucleosynthesis suggests that at least two nuclei represent the best candidates for the source of neutrons: ^{13}C and ^{22}Ne , which produce neutrons, respectively, via the $^{13}\text{C}(\alpha, n)^{16}\text{O}$ and via the $^{22}\text{Ne}(\alpha, n)^{25}\text{Mg}$ reactions [119]. Depending on the dominant neutron source, a different s-element pattern is expected. This is due to the fact that the $^{13}\text{C}(\alpha, n)^{16}\text{O}$ reaction is activated at temperatures around 0.9×10^8 K, typical of low-mass stars, while the ^{22}Ne neutron source can only be efficient in intermediate mass AGB stars where the temperatures are higher [120].

In the case of the $^{13}\text{C}(\alpha, n)^{16}\text{O}$ reaction, at low energies, the S-factor is dominated by the contribution of the near threshold resonance at 4.7 keV due to the 6.364 MeV level of ^{17}O , having $\Gamma_n = 136 \pm 5$ keV [121]. At the lowest energies, direct data, ending up around 280 keV, have to be corrected for atomic electron screening determining an enhancement of less than 20% for the lowest-energy data point. Therefore, potential systematic errors might be introduced in the evaluation of the bare-nucleus astrophysical factor [25]. As it allows us to determine the resonance parameters even for sub-threshold energies, the THM is suited to investigate the $^{13}\text{C}(\alpha, n)^{16}\text{O}$ reaction [122]. For such a reason, an experiment devoted to study the $^{13}\text{C}({}^6\text{Li}, n)^{16}\text{O}^2\text{H}$ reaction was performed at Florida State University. The Tandem-LINAC facility delivered a ${}^6\text{Li}$ beam at 7.82 MeV impinging onto 99% ^{13}C enriched foils. The data analysis, described in details in [123], clearly shows the presence of several resonances in the $^{13}\text{C}-\alpha$ relative energy spectrum at ~ -3 keV, ~ 810 keV, and ~ 1020 keV. In particular, the presence of a resonance located at 4.7 keV has been observed for the first time in the $^{13}\text{C}(\alpha, n)^{16}\text{O}$ reaction, as it lies at ultra low energies. This allowed us

to calculate the $S(E)$ -factor reported in Figure 10 with the blue line. The upper and lower blue lines set the recommended range allowed for by the statistical, normalization, and data reduction uncertainties [124]. For comparison, different available direct data set are reported in the same picture: data by [125–130] are represented by green, brown, orange, red, black, and open points, respectively.

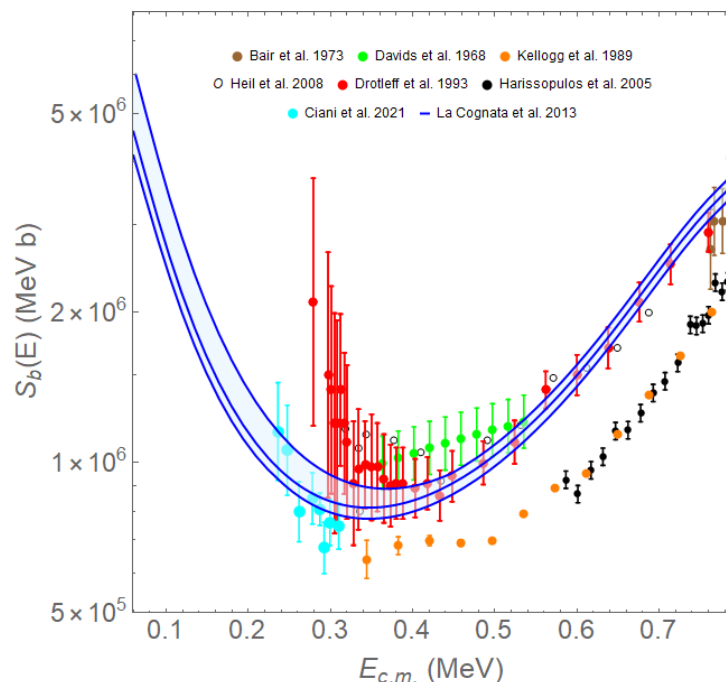


Figure 10. THM $S(E)$ -factor for the $^{13}\text{C}(\alpha,n)^{16}\text{O}$ reaction (blue line and blue band) compared with direct data available in the literature (see text for details).

Recently, the direct measurement performed at low energies by the LUNA collaboration [131] confirmed once again the results obtained with the THM approach. Those data are reported in Figure 10 with the cyan solid points.

7. Neutron Poison Reactions: The $^{17}\text{O}(n,\alpha)^{14}\text{C}$ and the $^{14}\text{N}(n,p)^{14}\text{C}$

Since light nuclei are relatively abundant with respect to heavier ones, a large fraction of the neutrons produced by the $^{13}\text{C}(\alpha,n)^{16}\text{O}$ and $^{22}\text{Ne}(\alpha,n)^{25}\text{Mg}$ reactions are captured by light nuclei and removed from the s -process nucleosynthesis path [132].

Indeed, the ignition of the $^{16}\text{O}(n,\gamma)^{17}\text{O}$ reaction is expected due to the presence of oxygen from the CNO cycle, making this reaction an important neutron poison reaction [133]. The produced ^{17}O can experience both (α,n) or (n,α) reactions; the $^{17}\text{O}(\alpha,n)^{20}\text{Ne}$ reaction represents a recycling channel for neutrons while the $^{17}\text{O}(n,\alpha)^{14}\text{C}$ reaction is a neutron-absorbing reaction [134]. Therefore, the knowledge of the ratio between the cross section of these processes is important to determine the overall neutron flux available for the subsequent s -process. In this framework, the $^{17}\text{O}(n,\alpha)^{14}\text{C}$ reaction has been extensively studied by different authors by means of direct experiments and by applying the detailed balance principle to the inverse reaction [135–139]. These measurements have shown the population of two excited states at 8213 keV and 8282 keV and the contribution of a sub-threshold level at 8038 keV, while no evidence for the 8125 keV level is present [140]. Indeed, as this resonance is populated in f -wave, its contribution is suppressed by the centrifugal barrier. Moreover, disagreement among the different data sets are still present, clearly causing a difference in the calculated total reaction rate of about a factor of 2.5–3 in the astrophysically relevant temperature region [138].

For all these reasons, a detailed measurement of the cross section in the energy range up to a few hundred keV was performed by applying the THM to the $^2\text{H}(^{17}\text{O},\alpha)^{14}\text{C}$ three-

body reaction [50,141]. Two experiments were performed: The first one at the INFN-LNS in Catania, Italy and the second one at the ISNAP of the University of Notre Dame, USA. A ^{17}O beam of 41(43.5) MeV was delivered onto a CD_2 target in the LNS (ISNAP) experiment. After the reaction channel selection and following the procedure described in [50,141] to probe the presence of a QF reaction process, the HOES cross section of the $^{17}\text{O}(n,\alpha)^{14}\text{C}$ reaction was extracted. Finally, good agreement between the two THM measurements, within the experimental uncertainties, allowed us to take the average of the two data cross section sets, weighting over the respective errors, to improve the statistical precision.

The experimental data were normalized to the available direct measurements [138], integrated over the angular distribution, and fitted following the modified R-matrix approach in order to calculate the reduced γ -widths of the excited levels. Thus, the calculated reaction rate is shown in Figure 11 with a black line, while the red band highlights the region allowed by uncertainties (statistical and normalization). In comparison, the reaction rate from [136] (red line) and [138] (blue line) are reported.

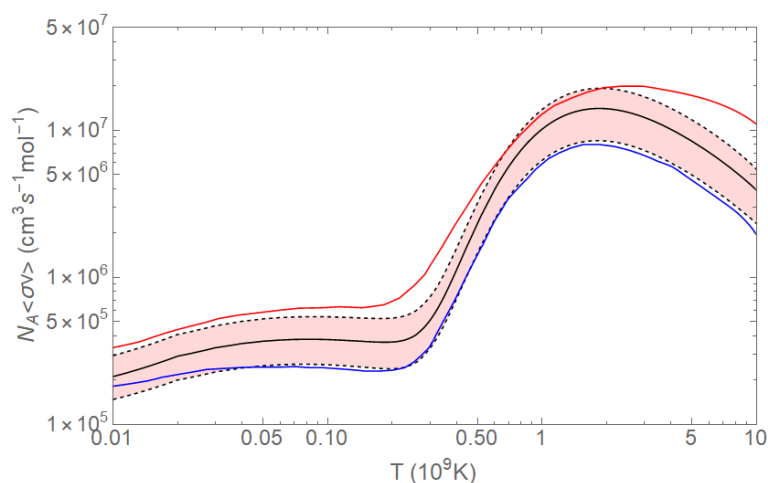


Figure 11. THM reaction rate for the $^{17}\text{O}(n,\alpha)^{14}\text{C}$ reaction (black line) in comparison with the ones available in the literature (see text for details).

From such a measurement, it was possible to excite the sub-threshold level centered at -7 keV in the center-of-mass system corresponding to the 8.039 MeV level of ^{18}O , which is important to determine the $^{17}\text{O}(n,\alpha)^{14}\text{C}$ reaction rate. In addition, it was found that the resonance corresponding to the 8.213 MeV level is better reproduced by adopting an angular momentum $l = 2$ instead of $l = 0$, as assumed in the past [135]. This result triggered the need for a new experiment with an improved detection setup and a wider angular coverage, whose analysis is still ongoing [142]. Finally, the use of the deuteron as a source of virtual neutrons allows us to populate the level centered at 75 keV in the ^{17}O -n center-of-mass system, corresponding to the 8.121 MeV level of ^{18}O . Due to its J^π assignment ($J^\pi = 5^-$), the population of such a level is suppressed in direct measurements because of its $l = 3$ angular momentum. The application of the modified R-matrix approach made it possible to measure the neutron and alpha partial widths that are in agreement with the ones available in the literature, while these partial widths were extracted for the first time in the case of the 8.125 MeV level. Therefore, extensive calculations are being undergone to understand the consequences of the present results on astrophysics.

In conclusion, the $^{14}\text{N}(n,p)^{14}\text{C}$ reaction also plays an important role in the s-process of nucleosynthesis: ^{14}N is very abundant since it is a dominant product of hydrogen-burning in the CNO cycle, the stage prior to the s-process. Thus, with its relatively high cross section, this reaction can act as a strong neutron poison in the reaction chain to heavier elements. Moreover, ^{14}N is of crucial importance in the nucleosynthetic origin of fluorine, whose only stable isotope is ^{19}F . The He-burning shell in asymptotic giant branch stars is thought to be the most likely site for the synthesis of fluorine, mainly through the nuclear

chain $^{14}\text{N}(\alpha, \gamma)^{18}\text{F}(\beta^+) ^{18}\text{O}(\text{p}, \alpha)^{15}\text{N}(\alpha, \gamma)^{19}\text{F}$. In this sense, the $^{14}\text{N}(\text{n}, \text{p})^{14}\text{C}$ reaction plays a key role because of its double effect of removing neutrons and producing protons. In addition, the protons can trigger the $^{18}\text{O}(\text{p}, \alpha)^{15}\text{N}$ or the $^{13}\text{C}(\text{p}, \gamma)^{14}\text{N}$ reactions, being the last one in competition with the $^{13}\text{C}(\alpha, \text{n})^{16}\text{O}$ reaction [73].

The first direct measurement of the stellar $^{14}\text{N}(\text{n}, \text{p})^{14}\text{C}$ cross section was done by [143]. Their result for the reaction rate was about a factor of three smaller than the rate used in most of the previous s-process calculations. It was also 2–3 times smaller than rates estimated from the inverse reaction and extrapolations from the thermal cross section, for which an evaluated value of 1.83 b was adopted. Measurements performed from thermal neutron energy up to 35 keV [144,145] found clear evidence for a $1/v$ behavior of the $^{14}\text{N}(\text{n}, \text{p})^{14}\text{C}$ reaction cross section up to approximately 30 keV and their results for the stellar reaction rate at $kT = 525$ keV are also approximately a factor of 3 higher than reported by [143]. Measurements with quasimonoenergetic neutrons at 25 keV from [146] are in fair agreement with the results from [144,145] and with the estimates from the inverse reaction, since again the same thermal value was used for the normalization. Another direct measurement of the $^{14}\text{N}(\text{n}, \text{p})^{14}\text{C}$ stellar cross section at $kT = 525$ keV was done by [147]. They found a value approximately a factor of 2 higher than [143] and a rather good agreement with the other results. In 1999, new measurements at neutron energies of 35.8 and 67.1 keV by [148] support the previous measurements but have rather large (20% and 12%, respectively) uncertainties. In 2000, the $^{14}\text{N}(\text{n}_{th}, \text{p})^{14}\text{C}$ reaction cross section was determined at the high flux reactor of the ILL in Grenoble [149]: They determined an accurate value of (1.93 ± 0.05) b for the $^{14}\text{N}(\text{n}_{th}, \text{p})^{14}\text{C}$ cross section, that is in good agreement with some results present in literature, however differs by 10% with the lower extreme value.

For this reason, careful new evaluation is needed and the THM was applied to determine the cross section of the $^{14}\text{N}(\text{n}, \text{p})^{14}\text{C}$ reaction by selecting the QF contribution to the $^2\text{H}({}^{14}\text{N}, \text{p} \text{ }^{14}\text{C})\text{p}$ reaction. The experiment was performed at INFN-LNS where the SMP Tandem accelerator provided a 40 MeV ^{14}N beam on a deuterated polyethylene target (CD_2) of about $150 \mu\text{g}/\text{cm}^2$ was placed at 90° with respect to the beam axis. The data analysis is already ongoing and final results will be published in the near future.

8. Conclusions

Indirect THM and ANC methods have been successfully used in the last few decades for measuring astrophysically relevant nuclear reaction cross sections bypassing the typical experimental difficulties often affecting the direct measurements, thus avoiding the need of extrapolation. In this review, the theoretical frameworks on which the THM and ANC methods were founded and discussed together with their typical systematic uncertainties. The impact of the THM and ANC measurements of interest for AGB star nucleosynthesis was detailed thanks to the devoted studies performed so far. Among the THM and ANC studies, it is worth mentioning ongoing $^{14}\text{N}(\text{n}, \text{p})^{14}\text{C}$ reaction data analysis because of its significant role as “neutron poison” for heavy elements nucleosynthesis. By following the standard THM data analysis procedure described elsewhere [19], the selection of the QF mechanism could be accomplished by studying the experimental momentum distribution. Then, the astrophysically relevant two-body reaction cross section could be extracted and compared with the direct data available in the literature. Further ongoing study is related to the $^{23}\text{Na}(\text{p}, \alpha)^{20}\text{Ne}$ reaction, involved in intermediate-mass AGB-star nucleosynthesis. A devoted THM experiment has already been performed and the preliminary data partially discussed in [150]. Among future plans, we also aim to complement the study of the $^{23}\text{Na}(\text{p}, \alpha)^{20}\text{Ne}$ with the one related to the $^{23}\text{Na}(\text{p}, \gamma)^{24}\text{Mg}$ by performing a devoted ANC experiment.

Author Contributions: M.L.S. was responsible for the $^{17}\text{O}(p,\alpha)^{14}\text{N}$ and the $^{17}\text{O}(p,\gamma)^{18}\text{F}$ data analysis. Nuclear data of $^{18}\text{O}(p,\gamma)^{19}\text{N}$ were analyzed by V.B. and J.M., while $^{19}\text{F}(\alpha,p)^{22}\text{Ne}$ reaction was investigated by G.D. and R.G.P. Data of the $^{17}\text{O}(n,\alpha)^{14}\text{C}$ reaction were analyzed by G.L.G., M.G., L.L. and A.A.O., M.L.C. was responsible for the $^{18}\text{O}(p,\alpha)^{15}\text{N}$, $^{15}\text{N}(p,\alpha)^{12}\text{C}$, $^{19}\text{F}(p,\alpha)^{16}\text{O}$, and $^{13}\text{C}(\alpha,n)^{16}\text{O}$ data analysis. Nuclear data of $^{14}\text{N}(n,p)^{14}\text{C}$ were analyzed by M.L.S. and L.L., while O.T. contributed significantly to the data analysis of $^{19}\text{F}(p,\alpha)^{16}\text{O}$ and $^{13}\text{C}(\alpha,n)^{16}\text{O}$. I.I. performed the data analysis of $^{19}\text{F}(p,\alpha)^{16}\text{O}$. M.L.S., G.D., G.L.G. and G.G.R. wrote the paper while S.C., D.L., S.R., R.S. and A.T. participated to the above experiments and contributed to the data analysis as well as the review of the paper. All authors have read and agreed to the published version of the manuscript.

Funding: This research was funded by “Programma ricerca di ateneo UNICT 2020-22 linea2 (PIA.CE.RI 2020-22)” and by “Starting grant 2020” of the University of Catania. J.M., V.B., and G.D. were supported by grant MEYS Czech Republic under the project SPIRAL2-CZ, EF16_013/0001679. D.L. was financially supported by: MIUR-Ministero dell’Istruzione, dell’Università e della Ricerca (Italian Ministry of Education, University and Research), PON R& 2014-2020 - AIM (Attraction and International Mobility), project AIM18487014-3.

Institutional Review Board Statement: Not applicable.

Informed Consent Statement: Not applicable.

Data Availability Statement: Datasets are available upon request directly to the authors.

Acknowledgments: The authors acknowledge Sara Palmerini for fruitful discussions during the writing of the present paper.

Conflicts of Interest: The authors declare that the research was conducted in the absence of any commercial or financial relationships that could be construed as a potential conflict of interest.

Note

- ¹ A third run was performed at the Nuclear Physics Institute of ASCR Czech Republic for studying the $^{19}\text{F}(^3\text{He},\alpha\ ^{16}\text{O})d$ process in view of polar invariance THM studies [106,107].

References

- Herwig, F. Evolution of Asymptotic Giant Branch Stars Formation *Annu. Rev. Astron. Astroph.* **2005**, *43*, 435. [[CrossRef](#)]
- Iliadis C. *Nuclear Physics of Stars*; Wiley-VCH: Weinheim, Germany, 2007
- Busso, M.; Gallino, R.; Wasserburg, G.J. Nucleosynthesis in Asymptotic Giant Branch Stars: Relevance for Galactic Enrichment and Solar System Formation *Annu. Rev. Astron. Astroph.* **1999**, *37*, 239. [[CrossRef](#)]
- Cristallo, S.; La Cognata, M.; Massimi, C.; Best, A.; Palmerini, S.; Straniero, O.; Trippella, O.; Busso, M.; Ciani, G.F.; Mingrone, F.; et al.; The Importance of the $^{13}\text{C}(\alpha,n)^{16}\text{O}$ Reaction in Asymptotic Giant Branch Stars. *Astroph. J.* **2018**, *859*, 14. [[CrossRef](#)]
- Palmerini, S.; Trippella, O.; Busso, M.; Vescovi, D.; Petrelli, M.; Zucchini, A.; Frondini, F. s-Processing from MHD-induced mixing and isotopic abundances in presolar SiC grains. *Geochim. Cosmochim. Acta* **2018**, *221*, 21. [[CrossRef](#)]
- Busso, M.; Vescovi, D.; Palmerini, S.; Cristallo, S.; Antonuccio-Delogu, V. s-processing in AGB Stars Revisited. III. Neutron Captures from MHD Mixing at Different Metallicities and Observational Constraints. *Astroph. J.* **2021**, *908*, 55. [[CrossRef](#)]
- Woodsley, S.E.; Haxton, W.C. Supernova neutrinos, neutral currents and the origin of fluorine. *Nature* **1988**, *334*, 45. [[CrossRef](#)]
- Goriely, S.E.; Jorissen, A.; Arnould, M. On the Mechanism of ^{19}F Production. In Proceedings of the 5th Workshop on Nuclear Astrophysics, Tegernsee, Germany, 30 January–4 February 1989.
- Meynet, G.; Arnould, M. Synthesis of ^{19}F in Wolf-Rayet stars. *Astron. Astrophys.* **2000**, *355*, 176.
- Palacios, A.; Arnould, M.; Meynet, G. The thermonuclear production of ^{19}F by Wolf-Rayet stars revisited. *Astron. Astrophys.* **2005**, *443*, 243. [[CrossRef](#)]
- Longland, R.; Lorén-Aguilar, P.; José, J.; García-Berro, E.; Althaus, L.G.; Isern, J. Nucleosynthesis during the Merger of White Dwarfs and the Origin of R Coronae Borealis Stars. *Astrophys. J. Lett.* **2011**, *737*, L34. [[CrossRef](#)]
- Vescovi, D.; Cristallo, S.; Palmerini, S.; Abia, C.; Busso, M. Magnetic-buoyancy-induced mixing in AGB stars: Fluorine nucleosynthesis at different metallicities. *Astron. Astrophys.* **2021**, *652*, 7. [[CrossRef](#)]
- Lucatello, S.; Masseron, T.; Johnson, J.A.; Pignatari, M.; Herwig, F. Fluorine and Sodium in C-rich Low-metallicity Stars. *Astrophys. J.* **2011**, *729*, 1. [[CrossRef](#)]
- Lattanzio, J.C.; Frost, C.A.; Cannon, R.C.; Wood, P.R. Hot Bottom Burning Nucleosynthesis in 6 Msolar Stellar Models. *Nuc. Phys. A* **1997**, *621*, 435. [[CrossRef](#)]
- Wasserburg, G.J.; Boothroyd, A.I.; Sackmann, I.-J. Deep Circulation in Red Giant Stars: A Solution to the Carbon and Oxygen Isotope Puzzles? *Astroph. J. Lett.* **1995**, *447*, 37. [[CrossRef](#)]

16. Palmerini, S.; Trippella, O.; Busso, M. A deep mixing solution to the aluminum and oxygen isotope puzzles in pre-solar grains. *Mon. Not. R. Astron. Soc.* **2017**, *467*, 1193.
17. Lugaro, M.; Karakas, A.I.; Bruno, C.G.; Aliotta, M.; Nittler, L.R.; Bemmerer, D.; Best, A.; Boeltzig, A.; Broggini, C.; Cacioli, A.; et al. Origin of meteoritic stardust unveiled by a revised proton-capture rate of ^{17}O . *Nat. Astron.* **2017**, *1*, 0027. [[CrossRef](#)]
18. Palmerini, S.; Cristallo, S.; Busso, M.; La Cognata, M.; Sergi, M.L.; Vescovi, D. Low mass stars or intermediate mass stars? The stellar origin of presolar oxide grains revealed by their isotopic composition. *Front. Astron. Space Sci.* **2020**, *7*, 103. [[CrossRef](#)]
19. Tribble, R.E.; Bertulani, C.A.; Mukhamedzhanov, A.M.; Spitaleri, C. Indirect techniques in nuclear astrophysics: A review. *Rep. Prog. Phys.* **2014**, *77*, 106901. [[CrossRef](#)]
20. Spitaleri, C.; La Cognata, M.; Lamia, L.; Pizzone, R.G.; Tumino, A. Astrophysics studies with the Trojan Horse Method. *Eur. Phys. J. A* **2019**, *55*, 161. [[CrossRef](#)]
21. Tumino, A.; Bertulani, A.C.; La Cognata, M.; Lamia, L.; Pizzone, R.G.; Romano, S.; Typel, S. The Trojan Horse Method: A Nuclear Physics Tool for Astrophysics. *Ann. Rev. Nuc. Part. Sci.* **2021**, *71*, 345–376 [[CrossRef](#)]
22. Blokhintsev, L.D.; Borbely, I.; Dolinskii, E.I. Nuclear vertex constants. *Sov. J. Part. Nucl.* **1977**, *8*, 485.
23. Mukhamedzhanov, A.M.; Timofeyuk, N.K. Astrophysical S-factor for the reaction $^7\text{Be}+p\rightarrow^8\text{B}+\gamma$. *J. Exp. Theor. Phys. Lett.* **1990**, *51*, 282.
24. Xu, H.M.; Gagliardi, C.A.; Tribble, R.E.; Mukhamedzhanov, A.M.; Timofeyuk, N.K. Overall Normalization of the Astrophysical S Factor and the Nuclear Vertex Constant for $^7\text{Be}(p,\gamma)^8\text{B}$ Reactions. *Phys. Rev. Lett.* **1994**, *73*, 2027. [[CrossRef](#)]
25. Rolfs, C.E.; Rodney, W.S. *Cauldrons in the Cosmos*; The University of Chicago Press: Chicago, IL, USA, 1988.
26. Jain, M.; Roos, P.G.; Pugh, H.G.; Holmgren, H.D. The $(p,p\alpha)$ and $(\alpha, 2\alpha)$ reactions on ^6Li and ^7Li at 60 MeV. *Nucl. Phys. A* **1970**, *153*, 49. [[CrossRef](#)]
27. Tumino, A.; Spitaleri, C.; Mukhamedzhanov, A.; Rapisarda, G.G.; Campajola, L.; Cherubini, S.; Crucillà, V.; Elekes, Z.; Fülöp, Z.; Gialanella, L.; et al. Off-energy-shell p-p scattering at sub-Coulomb energies via the Trojan horse method. *Phys. Rev. C* **2008**, *78*, 064001. [[CrossRef](#)]
28. Dolinsky, E.I.; Dzhamalov, P.O.; Mukhamedzhanov, A.M. Peripheral-Model Approach to Stripping into Resonant States. *Nucl. Phys. A* **1973**, *202*, 97. [[CrossRef](#)]
29. Mukhamedzhanov, A.M.; Blokhintsev, L.D.; Irgaziev, B.F.; Kadyrov, A.S.; La Cognata, M.; Spitaleri, C.; Tribble, R.E. Trojan Horse as an indirect technique in nuclear astrophysics. *J. Phys. G Nucl. Part. Phys.* **2008**, *35*, 014016 [[CrossRef](#)]
30. La Cognata, M.; Spitaleri, C.; Mukhamedzhanov, A.M.; Irgaziev, B.; Tribble, R.E.; Banu, A.; Cherubini, S.; Coc, A.; Crucillà, V.; Goldberg, V.Z.; et al. A Measurement of the 20 and 90 keV Resonances in the $^{18}\text{O}(p,\alpha)^{15}\text{N}$ Reaction via the Trojan Horse Method. *Phys. Rev. Lett.* **2008**, *101*, 152501. [[CrossRef](#)]
31. La Cognata, M.; Goldberg, V.Z.; Mukhamedzhanov, A.M.; Spitaleri, C.; Tribble, R.E. Improved determination of the astrophysical S(O) factor of the $^{15}\text{N}(p,\alpha)^{12}\text{C}$ reaction. *Phys. Rev. C* **2009**, *80*, 012801. [[CrossRef](#)]
32. La Cognata, M.; Spitaleri, C.; Mukhamedzhanov, A.; Banu, A.; Cherubini, S.; Coc, A.; Crucillà, V.; Goldberg, V.; Gulino, M.; Irgaziev, B.; et al. A Novel Approach to Measure the Cross Section of the $^{18}\text{O}(p,\alpha)^{15}\text{N}$ Resonant Reaction in the 0–200 keV Energy Range. *Astrophys. J.* **2010**, *708*, 796. [[CrossRef](#)]
33. La Cognata, M.; Spitaleri, C.; Mukhamedzhanov, A.; Goldberg, V.; Irgaziev, B.; Lamia, L.; Pizzone, R.G.; Sergi, M.L.; Tribble, R.E. DWBA momentum distribution and its effect on THM. *Nucl. Phys. A* **2010**, *834*, 658. [[CrossRef](#)]
34. Lamia, L.; La Cognata, M.; Spitaleri, C.; Irgaziev, B.; Pizzone, R.G. Influence of the d-state component of the deuteron wave function on the application of the Trojan horse method. *Phys. Rev. C* **2012**, *85*, 025805. [[CrossRef](#)]
35. Pizzone, R.G.; Spitaleri, C.; Cherubini, S.; La Cognata, M.; Lamia, L.; Miljanic, D.; Musumarra, A.; Romano, S.; Tumino, A.; Tudisco, S.; et al. Influence of the α -d motion in ^6Li on Trojan Horse applications. *Phys. Rev. C* **2005**, *71*, 058801. [[CrossRef](#)]
36. Tumino, A.; Spartá, R.; Spitaleri, C.; Mukhamedzhanov, A.M.; Typel, S.; Pizzone, R.G.; Tognelli, E.; Degl'Innocenti, S.; Burjan, V.; Kroha, V.; et al. New determination of the $^2\text{H}(d,p)^3\text{H}$ and $^2\text{H}(d,n)^3\text{He}$ reaction rates at astrophysical energies. *Astrophys. J.* **2014**, *785*, 96. [[CrossRef](#)]
37. Tumino, A.; Spitaleri, C.; La Cognata, M.; Cherubini, S.; Guardo, G.L.; Gulino, M.; Hayakawa, S.; Indelicato, I.; Lamia, L.; Petrascu, H.; et al. An increase in the $^{12}\text{C}+^{12}\text{C}$ fusion rate from resonances at astrophysical energies. *Nature* **2018**, *557*, 687. [[CrossRef](#)] [[PubMed](#)]
38. Tumino, A.; Spitaleri, C.; Mukhamedzhanov, A.; Rapisarda, G.G.; Cherubini, S.; Crucillà, E.Z.; Fülöp, Z.; Gulino, M.; Gyürky, G. Suppression of the Coulomb interaction in the Off-Energy-Shell p-p scattering from the $p+d\rightarrow p+p+n$ Reaction. *Phys. Rev. Lett.* **2007**, *98*, 252502. [[CrossRef](#)]
39. Spitaleri, C.; Bertulani, C.A.; Fortunato, L.; Vitturi, A. The electron screening puzzle and nuclear clustering. *Phys. Lett. B* **2016**, *755*, 275. [[CrossRef](#)]
40. Pizzone, R.G.; Bertulani, C.A.; Lamia, L.; La Cognata, M.; Sergi, M.L.; Spartá, R.; Tumino, A. Clusters and their fundamental role for Trojan Horse Method. *Eur. Phys. J. A*, **2020**, *56*, 283. [[CrossRef](#)]
41. Pizzone, R.G.; Spartá, R.; Bertulani, C.A.; Spitaleri, C.; La Cognata, M.; Lalmansingh, L.; Lamia, L.; Mukhamedzhanov, A.; Tumino, A. Big Bang Nucleosynthesis revisited via Trojan Horse Method measurements. *Astrophys. J.* **2014**, *786*, 112. [[CrossRef](#)]
42. Pizzone, R.G.; Spampinato, C.; Spartá, R.; Couder, M.; Tan, W.; Burjan, V.; D'Agata, G.; Guardo, G.L.; La Cognata, M.; Lamia, L.; et al. Indirect measurement of the $^3\text{He}(n,p)^3\text{H}$ reaction cross section at Big Bang energies. *Eur. Phys. J.* **2020**, *A56*, 199. [[CrossRef](#)]
43. Aliotta, M.; Spitaleri, C.; Lattuada, M.; Musumarra, A.; Pizzone, R.G.; Tumino, A.; Rolfs, C.; Strieder, F. Improved information on electron screening in $^7\text{Li}(p,\alpha)\alpha$ using the Trojan-horse method. *Eur. Phys. J. A* **2000**, *9*, 435. [[CrossRef](#)]

44. Lamia, L.; Spitaleri, C.; La Cognata, M.; Palmerini, S.; Pizzone, R.G. Recent evaluation of the ${}^7\text{Li}(p,\alpha){}^4\text{He}$ reaction rate at astrophysical energies via the Trojan Horse Method. *Astron. Astrophys.* **2012**, *541*, A158. [[CrossRef](#)]
45. Romano, S.; Lamia, L.; Spitaleri, C.; Li, C.; Cherubini, S.; Gulino, M.; La Cognata, M.; Pizzone, R.G.; Tumino, A. Study of the ${}^9\text{Be}(p,\alpha){}^6\text{Li}$ reaction via the Trojan Horse Method. *Eur. Phys. J. A* **2006**, *27*, 221. [[CrossRef](#)]
46. Lamia, L.; Spitaleri, C.; Tognelli, E.; Degl'Innocenti, S.; Pizzone, R.G.; Moroni, P.G.P. Astrophysical impact of the updated ${}^9\text{Be}(p,\alpha){}^6\text{Li}$ and ${}^{10}\text{B}(p,\alpha){}^7\text{Be}$ reaction rates as deduced by THM. *Astrophys. J.* **2015**, *811*, 99. [[CrossRef](#)]
47. Cvetinović, A.; Spitaleri, C.; Spartá, R.; Rapisarda, G.G.; Puglia, S.M.R.; La Cognata, M.; Cherubini, S.; Guardo, G.L.; Gulino, M.; Lamia, L.; et al. Trojan horse measurement of the ${}^{10}\text{B}(p,\alpha_0){}^7\text{Be}$ cross section in the energy range from 3 keV to 2.2 MeV. *Phys. Rev. C* **2018**, *97*, 065801. [[CrossRef](#)]
48. Rapisarda, G.G.; Spitaleri, C.; Cvetinović, A.; Spartá, R.; Cherubini, S.; Guardo, G.L.; Gulino, M.; La Cognata, M.; Lamia, L.; Pizzone, R.G.; et al. Study of the ${}^{10}\text{B}(p,\alpha_1){}^7\text{Be}$ reaction by means of the Trojan Horse Method. *Eur. Phys. J. A* **2018**, *54*, 189. [[CrossRef](#)]
49. Sergi, M.L.; Guardo, G.L.; La Cognata, M.; Gulino, M.; Mrázek, J.; Palmerini, S.; Spitaleri, C.; Wiescher, M. Indirect measurements of n- and p- induced reactions of astrophysical interest on oxygen isotopes. *Front. Astron. Space Sci.* **2020**, *7*, 60. [[CrossRef](#)]
50. Guardo, G.L.; Spitaleri, C.; Lamia, L.; Gulino, M.; La Cognata, M.; Tang, X.; deBoer, R.; Fang, X.; Goldberg, V.; Mrázek, J.; et al. Assessing the near threshold cross section of the ${}^{17}\text{O}(n,\alpha){}^{14}\text{C}$ reaction by means of the Trojan horse method. *Phys. Rev. C* **2017**, *95*, 025807. [[CrossRef](#)]
51. Guardo, G.L.; Spitaleri, C.; Lamia, L.; Spartá, R.; Carlin, N.; Cherubini, S.; Gimenez Del Santo, G.; Indelicato, I.; La Cognata, M.; Lattuada, D.; et al. The ${}^{10}\text{B}(n,\alpha){}^7\text{Li}$ cross sections at ultra-low energy through the Trojan Horse Method applied to the ${}^2\text{H}({}^{10}\text{B},\alpha){}^7\text{Li}$ reaction. *Eur. Phys. J. A* **2019**, *55*, 211. [[CrossRef](#)]
52. Pizzone, R.G.; Roeder, B.T.; McCleskey, M.; Trache, L.; Tribble, R.E.; Spitaleri, C.; Bertulani, C.A.; Cherubini, S.; Gulino, M.; Indelicato, I.; et al. Trojan Horse measurement of the ${}^{18}\text{F}(p,ff){}^{15}\text{O}$ astrophysical S(E)-factor. *Eur. Phys. J. A* **2016**, *52*, 24. [[CrossRef](#)]
53. La Cognata, M.; Pizzone, R.G.; José, J.; Hernanz, M.; Cherubini, S.; Gulino, M.; Rapisarda, G.G.; Spitaleri, C. A Trojan Horse approach to the production of ${}^{18}\text{F}$ in novae. *Astr. J.* **2017**, *65*, 846.
54. Lamia, L.; Spitaleri, C.; Bertulani, C.A.; Hou, S.Q.; La Cognata, M.; Pizzone, R.G.; Romano, S.; Sergi, M.L.; Tumino, A. On the Determination of the ${}^7\text{Be}(n,\alpha){}^4\text{He}$ Reaction Cross Section at BBN Energies. *Astrophys. J.* **2017**, *850*, 175. [[CrossRef](#)]
55. Lamia, L.; Mazzocco, M.; Pizzone, R.G.; Hayakawa, S.; La Cognata, M.; Spitaleri, C.; Bertulani, C.A.; Boiano, A.; Boiano, C.; Broggin, C.; et al. Cross-section measurement of the cosmologically relevant ${}^7\text{Be}(n,\alpha){}^4\text{He}$ reaction over a broad energy range in a single experiment. *Astrophys. J.* **2019**, *879*, 23. [[CrossRef](#)]
56. Burjan, V.; Hons, Z.; Kroha, V.; Mrázek, J.; Piskoř, Š.; Mukhamedzhanov, A.M.; Trache, L.; Tribble, R.E.; La Cognata, M.; Lamia, L.; et al. The determination of the astrophysical S-factor of the direct ${}^{18}\text{O}(p,\gamma){}^{19}\text{F}$ capture by the ANC method. *Eur. Phys. J. A* **2019**, *55*, 114. [[CrossRef](#)]
57. Mukhamedzhanov, A.M.; Burjan, V.; Gulino, M.; Hons, Z.; Kroha, V.; McCleskey, M.; Mrázek, J.; Nguyen, N.; Nunes, F.M.; Piskoř, Š.; et al. Asymptotic normalization coefficients from the ${}^{14}\text{C}(d,p){}^{15}\text{C}$ reaction. *Phys. Rev. C* **2011**, *84*, 024616. [[CrossRef](#)]
58. Kiss, G.G.; La Cognata, M.; Spitaleri, C.; Yarmukhamedov, R.; Wiedenhöver, I.; Baby, L.T.; Cherubini, S.; Cvetinovic, A.; D'Agata, G.; Figuera, P.; et al. Astrophysical S-factor for the ${}^3\text{He}(\alpha,\gamma){}^7\text{Be}$ reaction via the asymptotic normalization coefficient (ANC) method. *Phys. Lett. B* **2020**, *807*, 135606. [[CrossRef](#)]
59. Timofeyuk, N.K.; Johnson, R.C.; Mukhamedzhanov, A.M. Relation between Proton and Neutron Asymptotic Normalization Coefficients for Light Mirror Nuclei and its Relevance to Nuclear Astrophysics. *Phys. Rev. Lett.* **2003**, *91*, 232501. [[CrossRef](#)]
60. Trache, L.; Azhari, A.; Carstoiu, F.; Clark, H.L.; Gagliardi, C.A.; Liu, Y.W.; Mukhamedzhanov, A.M.; Tang, X.; Timofeyuk, N.K.; Tribble, R.E. Asymptotic normalization coefficients for ${}^8\text{B}\rightarrow{}^7\text{Be}+p$ from a study of ${}^8\text{Li}\rightarrow{}^7\text{Li}+p$. *Phys. Rev. C* **2003**, *67*, 062801. [[CrossRef](#)]
61. McCleskey, M.; Mukhamedzhanov, A.M.; Trache, L.; Tribble, R.E.; Banu, A.; Eremenko, V.; Goldberg, V.Z.; Lui, Y.-W.; McCleskey, E.; Roeder, B.T.; et al. Determination of the asymptotic normalization coefficients for ${}^{14}\text{C}+n\rightarrow{}^{15}\text{C}$, the ${}^{14}\text{C}(n,\gamma){}^{15}\text{C}$ reaction rate, and evaluation of a new method to determine spectroscopic factors. *Phys. Rev. C* **2014**, *89*, 044605. [[CrossRef](#)]
62. D'Agata, G.; Kilic, A.I.; Burjan, V.; Mrázek, J.; Glagolev, V.; Kroha, V.; Guardo, G.L.; La Cognata, M.; Lamia, L.; Palmerini, S.; et al. ${}^{26}\text{Si}(p,\gamma){}^{27}\text{P}$ direct proton capture by means of the asymptotic normalization coefficients method for mirror nuclei. *Phys. Rev. C* **2021**, *103*, 015806. [[CrossRef](#)]
63. Mukhamedzhanov, A.M.; Clark, H.L.; Gagliardi, C.A.; Liu, Y.W.; Trache, L.; Tribble, R.E.; Xu, H.M.; Zhou, X.G.; Burjan, V.; Cejpek, J.; et al. Asymptotic normalization coefficients for $10\text{B}\rightarrow{}^9\text{Be}+p$. *Phys. Rev. C* **1997**, *56*, 1302. [[CrossRef](#)]
64. Liu, Z.H.; Lin, C.J.; Zhang, H.Q.; Li, Z.C.; Zhang, J.S.; Wu, Y.W.; Yang, F.; Ruan, M.; Liu, J.C.; Li, S.Y.; et al. Asymptotic normalization coefficients and neutron halo of the excited states in ${}^{12}\text{B}$ and ${}^{13}\text{C}$. *Phys. Rev. C* **2001**, *64*, 034312. [[CrossRef](#)]
65. Mukhamedzhanov, A.M.; Nunes, F.M. Combined method to extract spectroscopic information. *Phys. Rev. C* **2005**, *72*, 017602. [[CrossRef](#)]
66. Belyaeva, T.L.; Perez-Torres, R.; Ogloblin, A.A.; Demyanova, A.S.; Ershov, S.N.; Goncharov, S.A. Determination of neutron halo radii in the first excited states of ${}^{13}\text{C}$ and ${}^{11}\text{Be}$ with the asymptotic normalization coefficients method. *Phys. Rev. C* **2014**, *90*, 064610. [[CrossRef](#)]
67. Yang, J.; Capel, P. Systematic analysis of the peripherality of the ${}^{10}\text{Be}(d,p){}^{11}\text{Be}$ transfer reaction and extraction of the asymptotic normalization coefficient of ${}^{11}\text{Be}$ bound states. *Phys. Rev. C* **2018**, *98*, 054602. [[CrossRef](#)]

68. Mukhamedzhanov, A.M.; Bém, P.; Burjan, V.; Gagliardi, C.A.; Goldberg, V.Z.; Hons, Z.; La Cognata, M.; Kroha, V.; Mrázek, J.; Novák, J.; et al. New astrophysical S factor for the $^{15}\text{N}(p, \gamma)^{16}\text{O}$ reaction via the asymptotic normalization coefficient (ANC) method. *Phys. Rev. C* **2008**, *78*, 015804. [[CrossRef](#)]
69. Kiss, G.G.; La Cognata, M.; Yarmukhamedov, R.; Tursunmakhmatov, K.I.; Wiedenhover, I.; Baby, L.T.; Cherubini, S.; Cvetinovic, A.; D'Agata, G.; Figuera, P.; et al. Indirect determination of the astrophysical S factor for the $^6\text{Li}(p, \gamma)^7\text{Be}$ reaction using the asymptotic normalization coefficient method. *Phys. Rev. C* **2021**, *104*, 015807. [[CrossRef](#)]
70. Burjan, V.; Mrázek, J.; D'Agata, G. ANC from experimental perspective. *Front. Astron. Space Sci.* **2020**, *7*, 562466, doi.org/10.3389/FSPAS.2020.562466 [[CrossRef](#)]
71. Palmerini, S.; Sergi, M.L.; La Cognata, M.; Lamia, L.; Pizzone, R.G.; Spitaleri, C. The RGB and AGB star nucleosynthesis in light of the recent $^{17}\text{O}(p, \alpha)^{14}\text{N}$ and $^{18}\text{O}(p, \alpha)^{15}\text{N}$ reaction rate determination. *Astrophys. J.* **2013**, *764*, 128. [[CrossRef](#)]
72. Chafa, A.; Tatischeff, V.; Aguer, P.; Barhoumi, S.; Coc, A.; Garrido, F.; Hernanz, M.; José, J.; Kiener, J.; Lefebvre-Schuhl, A.; et al. Experimental determination of the $^{17}\text{O}(p, \alpha)^{14}\text{N}$ and $^{17}\text{O}(p, \gamma)^{18}\text{F}$ reaction rates. *Phys. Rev. C* **2007**, *75*, 035810. [[CrossRef](#)]
73. Iliadis, C.; Longland, R.; Champagne, A.E.; Coc, A.; Fitzgerald, R. Charged-particle thermonuclear reaction rates: II. Tables and graphs of reaction rates and probability density functions. *Nucl. Phys. A* **2010**, *841*, 31–250. [[CrossRef](#)]
74. Newton, J.R.; Iliadis, C.; Champagne, A.E.; Longland, R.; Ugalde, C. Remeasurement of the 193 keV resonance in $^{17}\text{O}(p, \alpha)^{14}\text{N}$. *Phys. Rev. C* **2007**, *75*, 055808. [[CrossRef](#)]
75. Moazen, B.H.; Bardayan, D.W.; Blackmon, J.C.; Chae, K.Y.; Chipps, K.; Domizioli, C.P.; Fitzgerald, R.; Greife, U.; Hix, W.R.; Jones, K.L.; et al. Measurement of the 183 keV resonance in $^{17}\text{O}(p, \alpha)^{14}\text{N}$ using a novel technique. *Phys. Rev. C* **2007**, *75*, 065801. [[CrossRef](#)]
76. Sergi, M.L.; Spitaleri, C.; La Cognata, M.; Coc, A.; Mukhamedzhanov, A.; Burjan, S.V.; Cherubini, S.; Crucillá, V.; Gulino, M.; Hammache, F.; et al. New high accuracy measurement of the $^{17}\text{O}(p, \alpha)^{14}\text{N}$ reaction rate at astrophysical temperatures. *Phys. Rev. C* **2010**, *82*, 032801. [[CrossRef](#)]
77. Sergi, M.L.; Spitaleri, C.; La Cognata, M.; Lamia, L.; Pizzone, R.G.; Rapisarda, G.G.; Tang, X.D.; Bucher, B.; Couder, M.; Davies, P.; et al. Improvement of the high-accuracy $^{17}\text{O}(p, \alpha)^{14}\text{N}$ reaction rate measurement via the Trojan Horse method for application to ^{17}O nucleosynthesis. *Phys. Rev. C* **2015**, *91*, 065803. [[CrossRef](#)]
78. Di Leva, A.; Scott, D.A.; Caciolli, A.; Formicola, A.; Strieder, F.; Aliotta, M.; Anders, M.; Bemmerer, D.; Broggini, C.; Corvisiero, P.; et al. LUNA Collaboration Underground study of the $^{17}\text{O}(p, \gamma)^{18}\text{F}$ reaction relevant for explosive hydrogen burning. *Phys. Rev. C* **2014**, *89*, 015803. [[CrossRef](#)]
79. Bruno, C.G.; Scott, D.A.; Aliotta, M.; Formicola, A.; Best, A.; Boeltzig, A.; Bemmerer, D.; Broggini, C.; Caciolli, A.; Cavanna, F.; et al. Improved Direct Measurement of the 64.5 keV Resonance Strength in the $^{17}\text{O}(p, \alpha)^{14}\text{N}$ Reaction at LUNA. *Phys. Rev. Lett.* **2016**, *117*, 142502. [[CrossRef](#)]
80. Fox, C.; Iliadis, C.; Champagne, A.E.; Fitzgerald, R.P.; Longland, R.; Newton, J.; Pollanen, J.; Runkle, R. Thermonuclear reaction rate of $^{17}\text{O}(p, \gamma)^{18}\text{F}$. *Phys. Rev. C* **2005**, *71*, 055801. [[CrossRef](#)]
81. Adelberger, E.G.; García, A.; Hamish Robertson, R.G.; Snover, K.A.; Balantekin, A.B.; Heeger, K.; Ramsey-Musolf, M.J.; Bemmerer, D.; Junghans, A.; Bertulani, C.A.; et al. Solar fusion cross sections. II. The pp chain and CNO cycles. *Rev. Mod. Phys.* **2011**, *83*, 195. [[CrossRef](#)]
82. Angulo, C.; Arnould, M.; Rayet, M.; Descouvemont, P.; Baye, D.; Leclercq-Willain, C.; Coc, A.; Barhoumi, S.; Aguer, P.; Rolfs, C.; et al. compilation of charged-particle induced thermonuclear reaction rates. *Nucl. Phys. A* **1999**, *656*, 3–183. [[CrossRef](#)]
83. Champagne, A.E.; Pitt, M.L. The destruction of ^{18}O in red giants: A search for a sub-threshold resonance in the $^{18}\text{O}+p$ system. *Nuc. Phys. A* **1986**, *457*, 367. [[CrossRef](#)]
84. Wiescher M.; Becker, H.W.; Görres, J.; Kettner, K.U.; Trautvetter, H.P.; Kieser, W.E.; Rolfs, C.; Azuma, R.E.; Jackson, K.P.; Hammer, J.W.; Nuclear and astrophysical aspects of $^{18}\text{O}(p, \gamma)^{19}\text{F}$. *Nucl. Phys. A* **1980**, *349*, 165. [[CrossRef](#)]
85. La Cognata, M.; Spitaleri, C.; Mukhamedzhanov, A.M. Effect of the high-energy resonances on the $^{18}\text{O}(p, \alpha)^{15}\text{N}$ reaction rate at AGB and Post-AGB relevant temperatures. *Astrophys. J.* **2010**, *723*, 1512. [[CrossRef](#)]
86. Becker, H.W.; Bahr, M.; Berheide, M.; Borucki, L.; Buschmann, M.; Rolfs, C.; Roters, G.; Schmidt, S.; Schulte, W.H.; Mitchell, G.E.; et al. Hydrogen depth profiling using ^{18}O ions. *Z. Phys. A* **1995**, *351*, 453. [[CrossRef](#)]
87. Bruno, C.G.; Aliotta, M.; Descouvemont, P.; Best, A.; Davinson, T.; Bemmerer, D.; Boeltzig, A.; Broggini, C.; Caciolli, A.; Cavanna, F.; et al. Improved astrophysical rate for the $^{18}\text{O}(p, \alpha)^{15}\text{N}$ reaction by underground measurements. *Phys. Lett. B* **2019**, *790*, 237–242. [[CrossRef](#)]
88. Vogelaar, R.B.; Wang, T.R.; Kellog, S.E.; Kavanagh, R.W. Low-energy reaction yields for $^{18}\text{O}(p, \gamma)$ and $^{18}\text{O}(\alpha, \gamma)$. *Phys. Rev. C* **1990**, *42*, 753. [[CrossRef](#)] [[PubMed](#)]
89. Pantaleo, F.R.; Boeltzig, A.; Best, A.; Perrino, R.; Aliotta, M.; Balibrea-Correa, J.; Barile, F.; Bemmerer, D.; Broggini, C.; Bruno, C.G. Low-energy resonances in the $^{18}\text{O}(p, \gamma)^{19}\text{F}$ reaction. *Phys. Rev. C* **2021**, *104*, 025802. [[CrossRef](#)]
90. Buckner, M.Q.; Iliadis, C.; Cesaratto, J.M.; Howard, C.; Clegg, T.B.; Champagne, A.E.; Daigle, S. Thermonuclear reaction rate of $^{18}\text{O}(p, \gamma)^{19}\text{F}$. *Phys. Rev. C* **2012**, *86*, 065804. [[CrossRef](#)]
91. Vernotte, J.; Berrier-Ronsin, G.; Kalifa, J.; Tamisier, R. Optical model analysis of ^3He elastic scattering from s-d shell nuclei at 25 MeV. *Nucl. Phys. A* **1982**, *390*, 285. [[CrossRef](#)]
92. Trost, H.J.; Lezoch, P.; Strohmusch, U. Simple optical model treatment of the elastic ^3He scattering. *Nucl. Phys. A* **1987**, *462*, 333. [[CrossRef](#)]

93. Perey, C.M.; Perey, F.G. Compilation of phenomenological optical-model parameters 1954–1975. *At. Data Nucl. Data Tables* **1976**, *17*, 1–101. [[CrossRef](#)]
94. Brida, I.; Pieper, S.C.; Wiringa, R.B. Quantum Monte Carlo calculations of spectroscopic overlaps in $A \leq 7$ nuclei. *Phys. Rev. C* **2011**, *84*, 024319. [[CrossRef](#)]
95. Lugaro, M.; Ugalde, C.; Karakas, A.I.; Görres, J.; Wiescher, M.; Lattanzio, J.C.; Cannon, R.C. Reaction Rate Uncertainties and the Production of ^{19}F in Asymptotic Giant Branch Stars. *Astrophys. J.* **2004**, *615*, 934. [[CrossRef](#)]
96. Schardt, A.; Fowler, W.A.; Lauritsen, C.C.; The Disintegration of ^{15}N by Protons. *Phys. Rev.* **1952**, *86*, 527–535. [[CrossRef](#)]
97. Zyskind, J.L.; Parker, P.D. Remeasurement of the low-energy cross section for the $^{15}\text{N}(p,\alpha_0)^{12}\text{C}$ reaction. *Nucl. Phys. A* **1979**, *320*, 404–412. [[CrossRef](#)]
98. Redder, A.; Becker, H.W.; Lorenz-Wirzba, H.; Rolfs, C.; Schmalbrock, P.; Trautvetter, H.P. The $^{15}\text{N}(p,\alpha_0)^{12}\text{C}$ reaction at stellar energies. *Z. Phys. A* **1982**, *305*, 325–333. [[CrossRef](#)]
99. La Cognata, M.; Romano, S.; Spitaleri, C.; Cherubini, S.; Crucillá, V.; Gulino, M.; Lamia, L.; Pizzone, R.G.; Tumino, A.; Tribble, R.; et al. Astrophysical S(E) factor of the $^{15}\text{N}(p,\alpha)^{12}\text{C}$ reaction at sub-Coulomb energies via the Trojan horse method. *Phys. Rev. C* **2007**, *76*, 065804. [[CrossRef](#)]
100. Palmerini, S.; La Cognata, M.; Cristallo, S.; Busso, M. Deep Mixing in Evolved Stars. I. The Effect of Reaction Rate Revisions from C to A. *Astrophys. J.* **2011**, *729*, 3. [[CrossRef](#)]
101. Spyrou, K.; Chronidou, C.; Harissopulos, S.; Kossionides, S.; Paradellis, T.; Rolfs, C.; Schulte, W.H.; Borucki, L. The title of the cited article. *Eur. Phys. J. A* **2000**, *7*, 79–85. [[CrossRef](#)]
102. Breuer, G. Messung und Analyse von Winkelverteilung und Wirkungsquerschnitt der Reaktion $^{19}\text{F}(p,\alpha_0)^{16}\text{O}$ im Energiebereich 0.4 bis 0.72 MeV. *Z. Phys.* **1959**, *154*, 339–351. [[CrossRef](#)]
103. Lombardo, I.; Dell’Aquila, D.; Di Leva, A.; Indelicato, I.; La Cognata, M.; La Commara, M.; Ordine, A.; Rigato, V.; Romoli, M.; Rosato, E.; et al. Toward a reassessment of the $^{19}\text{F}(p,\alpha_0)^{16}\text{O}$ reaction rate at astrophysical temperatures. *Phys. Lett. B* **2015**, *748*, 178–182. [[CrossRef](#)]
104. La Cognata, M.; Mukhamedzhanov, A.M.; Spitaleri, C.; Indelicato, I.; Aliotta, M.; Burjan, V.; Cherubini, S.; Coc, A.; Gulino, M.; Hons, Z.; et al. The Fluorine Destruction in Stars: First Experimental Study of the $^{19}\text{F}(p,\alpha_0)^{16}\text{O}$ Reaction at Astrophysical Energies. *Astrophys. J. Lett.* **2011**, *739*, L54. [[CrossRef](#)]
105. Zhang, L.Y.; Su, J.; He, J.J.; Wiescher, M.; deBoer, R.J.; Kahl, D.; Chen, Y.J.; Li, X.Y.; Wang, J.G.; Zhang, L.; et al. Direct Measurement of the Astrophysical $^{19}\text{F}(p,\alpha\gamma)^{16}\text{O}$ Reaction in the Deepest Operational Underground Laboratory. *Phys. Rev. Lett.* **2021**, *127*, 152702. [[CrossRef](#)] [[PubMed](#)]
106. Pizzone, R.G.; Spitaleri, C.; Lamia, L.; Bertulani, C.A.; Mukhamedzhanov, A.M.; Blokhintsev, L.; Burjan, V.; Cherubini, S.; Hons, Z.; Kiss, G.G.; et al. Trojan horse particle invariance studied with the $^6\text{Li}(d,\alpha)^4\text{He}$ and $^7\text{Li}(p,\alpha)^4\text{He}$ reactions. *Phys. Rev. C* **2011**, *83*, 045801. [[CrossRef](#)]
107. Pizzone, R.G.; Spitaleri, C.; Bertulani, C.A.; Mukhamedzhanov, A.M.; Blokhintsev, L.; La Cognata, M.; Lamia, L.; Rinollo, A.; Spartá, R.; Tumino, A. Updated evidence of the Trojan horse particle invariance for the $^2\text{H}(d,p)^3\text{H}$ reaction. *Phys. Rev. C* **2013**, *87*, 025805. [[CrossRef](#)]
108. La Cognata, M.; Palmerini, S.; Spitaleri, C.; Indelicato, I.; Mukhamedzhanov, A.M.; Lombardo, I.; Trippella, O. Updated THM Astrophysical Factor of the $^{19}\text{F}(p,\alpha)^{16}\text{O}$ Reaction and Influence of New Direct Data at Astrophysical Energies. *Astroph. J.* **2015**, *805*, 128. [[CrossRef](#)]
109. Indelicato, I.; La Cognata, M.; Spitaleri, C.; Burjan, V.; Cherubini, S.; Gulino, M.; Hayakawa, S.; Hons, Z.; Kroha, V.; Lamia, L.; et al. New Improved Indirect Measurement of the $^{19}\text{F}(p,\alpha)^{16}\text{O}$ Reaction at Energies of Astrophysical Relevance. *Astroph. J.* **2017**, *845*, 19. [[CrossRef](#)]
110. Lombardo, I.; Dell’Aquila, D.; Campajola, L.; Rosato, E.; Spadaccini, G.; Vigilante, M. Analysis of the $^{19}\text{F}(p,\alpha_0)^{16}\text{O}$ reaction at low energies and the spectroscopy of ^{20}Ne . *J. Phys. G Nucl. Partic.* **2013**, *40*, 125102. [[CrossRef](#)]
111. Palmerini, S.; D’Agata, G.; La Cognata, M.; Indelicato, I.; Pizzone, R.G.; Trippella, O.; Vescovi, D. $^{19}\text{F}(p,\alpha)^{16}\text{O}$ and $^{19}\text{F}(\alpha,p)^{22}\text{Ne}$ Reaction Rate Measured via THM and Fluorine Nucleosynthesis in AGB stars. *J. Phys. Conf. Ser.* **2019**, *1308*, 012016. [[CrossRef](#)]
112. Cristallo, S.; Di Leva, A.; Imbriani, G.; Piersanti, L.; Abia, C.; Gialanella, L.; Straniero, O. Effects of nuclear cross sections on ^{19}F nucleosynthesis at low metallicities. *Astron. Astrophys.* **2014**, *570*, 46. [[CrossRef](#)]
113. Ugalde, C.; Azuma, R.E.; Couture, A.; Görres, J.; Lee, H.Y.; Stech, E.; Strandberg, E.; Tan, W.; Wiescher, M. Thermonuclear rate for the $^{19}\text{F}(\alpha,p)^{22}\text{Ne}$ reaction at stellar temperatures. *Phys. Rev. C* **2008**, *77*, 035801. [[CrossRef](#)]
114. Pizzone, R.G.; D’Agata, G.; La Cognata, M.; Indelicato, I.; Spitaleri, C.; Blagus, S.; Cherubini, S.; Figuera, P.; Grassi, L.; Guardo, G.L.; et al. First Measurement of the $^{19}\text{F}(\alpha,p)^{22}\text{Ne}$ Reaction at Energies of Astrophysical Relevance. *Astrophys. J.* **2017**, *836*, 57. [[CrossRef](#)]
115. D’Agata, G.; Pizzone, R.G.; La Cognata, M.; Indelicato, I.; Spitaleri, C.; Palmerini, S.; Trippella, O.; Vescovi, D.; Blagus, S.; Cherubini, S.; et al. The $^{19}\text{F}(\alpha,p)^{22}\text{Ne}$ Reaction at Energies of Astrophysical Relevance by Means of the Trojan Horse Method and Its Implications in AGB Stars. *Astrophys. J.* **2018**, *860*, 61. [[CrossRef](#)]
116. Trippella, O.; Busso, M.; Maiorca, E.; Käppler, F.; Palmerini, S. s–processing in AGB Stars revisited. I. Does the main component constrain the neutron source in the ^{13}C pocket? *Astrophys. J.* **2014**, *787*, 41. [[CrossRef](#)]
117. Burbidge, E.M.; Burbidge, G.R.; Fowler, W.A.; Hoyle, F. Synthesis of the Elements in Stars. *Rev. Mod. Phys.* **1957**, *29*, 547. [[CrossRef](#)]

118. Cameron, A.G.W. Origin of Anomalous Abundances of the Elements in Giant Stars. *Astron. J.* **1955**, *121*, 144. [[CrossRef](#)]
119. Cameron, A.G.W. New Neutron Sources of Possible Astrophysical Importance. *Astron. J.* **1960**, *65*, 485. [[CrossRef](#)]
120. Clayton, D.D.; Fowler, W.A.; Hull, T.E.; Zimmerman, B.A. Neutron capture chains in heavy element synthesis. *Ann. Phys.* **1961**, *12*, 331. [[CrossRef](#)]
121. Faestermann, T.; Mohr, P.; Hertenberg, R.; Wirth, H.-F. Broad levels in ^{17}O and their relevance for the astrophysical s-process. *Phys. Rev. C* **2015**, *92*, 052802(R). [[CrossRef](#)]
122. La Cognata, M.; Spitaleri, C.; Trippella, O.; Kiss, G.G.; Rogachev, G.V.; Mukhamedzhanov, A.M.; Avila, M.; Guardo, G.L.; Koshchiy, E.; Kuchera, A.; et al. Measurement of the -3 keV resonance in the reaction $^{13}\text{C}(\alpha, n)^{16}\text{O}$ of importance in the s-process. *Phys. Rev. Lett.* **2012**, *109*, 23. [[CrossRef](#)]
123. La Cognata, M.; Spitaleri, C.; Trippella, O.; Kiss, G.G.; Rogachev, G.V.; Mukhamedzhanov, A.M.; Avila, M.; Guardo, G.L.; Koshchiy, E.; Kuchera, A.; et al. On the measurement of the $^{13}\text{C}(\alpha, n)^{16}\text{O}$ S-Factor at negative energies and its influence on the s-process. *Astrophys. J.* **2013**, *777*, 143. [[CrossRef](#)]
124. Trippella, O.; La Cognata, M. Concurrent Application of ANC and THM to assess the $^{13}\text{C}(\alpha, n)^{16}\text{O}$ Absolute Cross Section at Astrophysical Energies and Possible Consequences for Neutron Production in Low-mass AGB Stars. *Astrophys. J.* **2017**, *837*, 41. [[CrossRef](#)]
125. Davids, C.N. A study of (α, n) reactions on ^9Be and ^{13}C at low energies. *Nucl. Phys. A* **1968**, *110*, 3. [[CrossRef](#)]
126. Bair, J.K.; Haas, F.X. Total Neutron Yield from the Reactions $^{13}\text{C}(\alpha, n)^{16}\text{O}$ and $^{17,18}\text{O}(\alpha, n)^{20,21}\text{Ne}$. *Phys. Rev. C* **1973**, *7*, 1356. [[CrossRef](#)]
127. Kellogg, S.; Vogelaar, R.; Kavanagh, R.W.; $^{13}\text{C}(\alpha, n)$ and $^{14}\text{C}(\text{p}, n)$: Astrophysical Neutron Sources and Sinks *BAPS* **1989**, *34*, 1192.
128. Drotleff, H.W.; Denker, A.; Knee, H.; Soine, M.; Wolf, G.; Hammer, J.W.; Greife, U.; Rolfs, C.; Trautvetter, H.P. Reaction Rates of the s-Process Neutron Sources $^{22}\text{Ne}(\alpha, n)^{25}\text{Mg}$ and $^{13}\text{C}(\alpha, n)^{16}\text{O}$. *Astrophys. J.* **1993**, *414*, 735. [[CrossRef](#)]
129. Harissopulos, S.; Becker, H.W.; Hammer, J.W.; Lagoyannis, A.; Rolfs, C.; Strieder, F. Cross section of the $^{13}\text{C}(\alpha, n)^{16}\text{O}$ reaction: A background for the measurement of geo-neutrinos. *Phys. Rev. C* **2005**, *72*, 062801(R). [[CrossRef](#)]
130. Heil, M.; Detwiler, R.; Azuma, R.E.; Couture, A.; Daly, J.; Görres, J.; Käppeler, F.; Reifarh, R.; Tischhauser, P.; Ugalde, C.; et al. The $^{13}\text{C}(\alpha, n)$ reaction and its role as a neutron source for the s process. *Phys. Rev. C* **2008**, *78*, 025803. [[CrossRef](#)]
131. Ciani, G.F.; Csedreki, L.; Rapagnani, D.; Aliotta, M.; Balibrea-Correa, J.; Barile, F.; Bemmerer, D.; Best, A.; Boeltzig, A.; Brogini, C.; et al. Direct Measurement of the $^{13}\text{C}(\alpha, n)^{16}\text{O}$ Cross Section into the s-Process Gamow Peak. *Phys. Rev. Lett.* **2021**, *127*, 152701. [[CrossRef](#)]
132. Käppeler, F.; Gallino, R.; Bisterzo, S.; Wako, A. The s-process: Nuclear physics, stellar models, and observations. *Rev. Mod. Phys.* **2011**, *83*, 157. [[CrossRef](#)]
133. Mohr, P.; Heinz, C.; Pignatari, M.; Dillmann, I.; Mengoni, A.; Käppeler, F. Re-evaluation of the $^{16}\text{O}(n, \gamma)^{17}\text{O}$ Cross Section at Astrophysical Energies and Its Role as a Neutron Poison in the s-process. *Astrophys. J.* **2016**, *827*, 29. [[CrossRef](#)]
134. Pignatari, M.; Gallino, R.; Heil, M.; Wiescher, M.; Käppeler, F.; Herwig, F.; Bisterzo, S. The weak s-process in massive stars and its dependence on the neutron capture cross sections. *Astrophys. J.* **2010**, *710*, 1557. [[CrossRef](#)]
135. Sanders, M.R. Study of the $^{14}\text{C}(\text{p}, n)^{14}\text{N}$ and $^{14}\text{C}(\alpha, n)^{17}\text{O}$ Reactions. *Phys. Rev.* **1956**, *104*, 1434. [[CrossRef](#)]
136. Koehler, P.E.; Graff, S.M. $^{17}\text{O}(n, \alpha)^{14}\text{C}$ cross section from 25 meV to approximately 1 MeV. *Phys. Rev. C* **1991**, *44*, 2788. [[CrossRef](#)] [[PubMed](#)]
137. Schatz, H.; Käppeler, F.; Koehler, P.E.; Wiescher, M.; Trautvetter, H.P. $^{17}\text{O}(n, \alpha)^{14}\text{C}$: Closure of a Primordial CNO Bi-Cycle? *Astrophys. J.* **1993**, *413*, 750. [[CrossRef](#)]
138. Wagemans, J.; Wagemans, C.; Goeminne, G.; Serot, O.; Loiselet, M.; Gaelens, M. The $^{17}\text{O}(n, \alpha)^{14}\text{C}$ reaction from subthermal up to approximately 350 keV neutron energy. *Phys. Rev. C* **2002**, *65*, 034614. [[CrossRef](#)]
139. Avila, M.L.; Rogachev, G.V.; Goldberg, V.Z.; Johnson, E.D.; Kemper, K.W.; Tchuvil'sky, Y.M.; Volya, A.S. α -cluster structure of ^{18}O . *Phys. Rev. C* **2014**, *90*, 024327. [[CrossRef](#)]
140. Ajzenberg-Selove, F. Energy levels of light nuclei $A = 18-20$. *Nuc. Phys. A* **1987**, *475*, 1-198. [[CrossRef](#)]
141. Gulino, M.; Spitaleri, C.; Tang, X.D.; Guardo, G.L.; Lamia, L.; Cherubini, S.; Bucher, B.; Burjan, V.; Couder, M.; Davies, P.; et al. Suppression of the centrifugal barrier effects in the off-energy-shell neutron+ ^{17}O interaction. *Phys. Rev. C* **2013**, *87*, 012801(R). [[CrossRef](#)]
142. Oliva, A.A.; Guardo, G.L.; Lamia, L.; Cherubini, S.; Cvetinovic, A.; D'Agata, G.; de Sereville, N.; Di Pietro, A.; Figuera, P.; Gulino, M.; et al. Study of the neutron-induced reaction $^{17}\text{O}(n, \alpha)^{14}\text{C}$ at astrophysical energies via the Trojan Horse Method. *Il Nuovo Cimento C* **2020**, *111*, 1-9 [[CrossRef](#)]
143. Brehm, K.; Becker, H.W.; Rolfs, C.; Trautvetter, H.P.; Käppeler, F.; Ratynski, W. The cross section of $^{14}\text{N}(n, p)^{14}\text{C}$ at stellar energies and its role as a neutron poison for S-process nucleosynthesis. *Z. Phys. A* **1988**, *330*, 167.
144. Koehler, P.E.; O'Brien, H.A. $^{14}\text{N}(n, p)^{14}\text{C}$ cross section from 61 meV to 34.6 keV and its astrophysical implications. *Phys. Rev. C* **1989**, *39*, 1655. [[CrossRef](#)] [[PubMed](#)]
145. Koehler, P.E. $^{14}\text{N}(n, p)^{14}\text{C}$ cross section near thermal energy. *Phys. Rev. C* **1993**, *48*, 439. [[CrossRef](#)] [[PubMed](#)]
146. Gledenov, Y.M.; Salatski, V.I.; Sedyshev, P.V.; Sedysheva, M.V.; Pshenichnyj, V.A.; Andrzejewski, J. Cross sections of the $^{14}\text{N}(n, p)^{14}\text{C}$ reaction at 24.5, 53.5 and 144 keV. *Z. Phys. A* **1994**, *348*, 199. [[CrossRef](#)]

147. Sanami, T.; Baba, M.; Matsuyama, I.; Matsuyama, S.; Kiyosumi, T.; Nauchi, Y.; Hirakawa, N. Measurement of $^{14}\text{N}(n,p)^{14}\text{C}$ cross section for $kT = 25.3$ keV Maxwellian neutrons using gridded ionization chamber. *Nuclear Instrum. Methods Phys. Res. A* **1997**, *394*, 368. [[CrossRef](#)]
148. Kii, T.; Shima, T.; Sato, H.; Baba, T.; Nagai, Y. Cross section of the $^{14}\text{N}(n,p)^{14}\text{C}$ reaction from 10 to 100 keV measured by a gas scintillation drift chamber *Phys. Rev. C* **1999**, *59*, 3397.
149. Wagemans, J.; Wagemans, C.; Goeminne, G.; Geltenbort, P. Experimental determination of the $^{14}\text{N}(n,p)^{14}\text{C}$ reaction cross section for thermal neutrons. *Phys. Rev. C* **2000**, *61*, 064601. [[CrossRef](#)]
150. D'Agata, G.; Pizzone, R.G.; La Cognata, M.; Indelicato, I.; Spitaleri, C.; Burjan, V.; Cherubini, C.; Di Pietro, A.; Guardo, G.L.; Gulino, M.; et al. The $^{19}\text{F}(\alpha,p)^{22}\text{Ne}$ and $^{23}\text{Na}(p,\alpha)^{20}\text{Ne}$ reaction in AGB nucleosynthesis via THM. *EPJ Web Conf.* **2018**, *184*, 02003. [[CrossRef](#)]